Synapses and Ca^{2+} activity in oligodendrocyte precursor cells predict where myelin sheaths form

Jiaxing Li[1, *], Tania Miramontes[1], Tim Czopka[2], Kelly Monk[1, *]

1 Vollum Institute, Oregon Health & Science University, Portland, OR, USA

2 Centre for Clinical Brain Sciences, University of Edinburgh, Edinburgh, UK

*Corresponding authors

SUMMARY

In the nervous system, only one type of neuron-glial synapse is known to exist: that between neurons and oligodendrocyte precursor cells (OPCs). Neuron-OPC synapses are thought to bridge neuronal activity to OPCs. However, their composition, assembly, downstream signaling, and *in vivo* functions remain largely unclear. Here, we use zebrafish to address these questions and identify postsynaptic molecules PSD-95 and Gephyrin in OPCs. They increase during early development and decrease upon OPC differentiation. PSD-95 and Gephyrin in OPCs are highly dynamic and frequently assemble at "hotspots." Gephyrin "hotspots" and synapse-associated Ca^{2+} activity in OPCs predict where myelin sheaths form in oligodendrocytes. Further analyses reveal that spontaneous synaptic release from neurons mediates most OPC Ca^{2+} activity, while evoked synaptic release contributes only in early development. Finally, disruption of the synaptic molecule Nlgn3 impairs OPC differentiation and myelination. Together, we propose that neuron-OPC synapses are dynamically assembled and predetermine myelination patterns through Ca^{2+} signaling.

45 **INTRODUCTION**

46 Oligodendrocyte precursor cells (OPCs) are a dynamic cell type in the central nervous system
47 (CNS) with frequent migration, proliferation, process remodeling, and differentiation. OPCs and
48 their interactions with neurons play important roles in CNS health and disease such as
49 myelination and remyelination[1], neural network remodeling[2], and glioma progression[3].
50 Synapses form between neurons (presynaptic) and OPCs (postsynaptic) and represent the only
51 type of glial synapse in the nervous system. The composition of neuron-OPC synapses is largely
52 unknown, with the exception of some synaptic receptors (*e.g.*, glutamatergic and GABAergic)
53 that were revealed by pharmacology and electrophysiology[4]. Neuron-OPC synapse assembly
54 and regulation *in vivo* are mysterious, due to a paucity of tools to label these structures.
55 Previous studies knocking down single synaptic receptor types found diverse and sometimes
56 conflicting effects on OPC development and myelination: blocking NMDA receptors reduced or
57 had no effect on myelination[5,6]; blocking GABA receptors enhanced or had no effect on OPC
58 proliferation[7,8]. This is possibly due to redundancy, as OPCs possess multiple synaptic receptors[4].
59 Therefore, our understanding of the functions of neuron-OPC synapses is incomplete.

60 OPCs are hypothesized to sense the "activity" of neurons through neuron-OPC synapses.
61 Several studies support this idea: neuronal activity can modulate OPC development and
62 myelination[9–13]; *ex vivo* rodent studies using axonal stimulation observed synapse-dependent
63 Ca^{2+} increases in oligodendrocyte lineage cells, mostly in somas[14–16]. However, the *in vivo*
64 relationship between neuronal activity, neuron-OPC synapses, and OPC Ca^{2+} activity without
65 exogenous stimulation is unknown. Furthermore, the role of synapses in forming microdomain
66 (MD) Ca^{2+} events in OPC processes[17,18] is not addressed.

67 Here we identify postsynaptic scaffold proteins membrane-associated guanylate
68 kinases (MAGUKs), PSD-95 (a MAGUK member), and Gephyrin in zebrafish OPCs. The
69 postsynaptic puncta number in OPCs increases during early development, reduces upon OPC
70 differentiation, and exhibits small differences across the CNS regions but no difference between
71 OPC subgroups. *In vivo* imaging of PSD-95 and Gephyrin puncta in OPCs reveals that the puncta
72 are highly dynamic, resulting in extensive synaptic coverage. Although dynamic, postsynaptic
73 puncta repeatedly assemble at approximately 10 hotspots per OPC. Gephyrin hotspots at the
74 OPC stage predict where myelin sheaths form at the oligodendrocyte stage, in a synaptic
75 release-dependent manner. Further analysis reveals that Ca^{2+} activity is associated with neuron-
76 OPC synapses and similarly predicts where myelin sheaths form. The majority of *in vivo* OPC
77 Ca^{2+} events occur in MDs, require spontaneous synaptic release and, during early development,
78 require evoked synaptic release from neurons. Finally, we find that disruption of *neuroligin3*
79 (*nlgn3*), a gene important for synapse structure and function, impairs OPC development and
80 myelination. Collectively, these results suggest that dynamically assembled neuron-OPC
81 synapses predetermine myelination patterns through spontaneous and evoked synaptic Ca^{2+}
82 signaling in OPCs.
83

84 ## RESULTS

85 **Postsynaptic organizers MAGUK/PSD-95 and Gephyrin are present in zebrafish spinal cord**
86 **OPCs**

87 Transcript expression of *psd-95/dlg4* (often associated with Glutamate receptors) and
88 *gephyrin* (often associated with GABA and Glycine receptors) were previously reported in OPCs

89 (Extended Data Fig. 1a-b)[17,19]. We detected the presence of MAGUK/PSD-95 and Gephyrin
90 puncta in zebrafish spinal cord OPCs using immunohistochemistry (IHC) at 3 days post-
91 fertilization (dpf) (Fig. 1a-c and Extended Data Fig. 1c-f). We identified 16.6 ± 2.5 MAGUK
92 puncta and 29 ± 3.1 Gephyrin puncta per OPC (Fig. 1d), which were localized to OPC somas and
93 processes (Extended Data Fig. 1g). Gephyrin antibody specificity was verified in zebrafish with
94 *gephyrin* CRISPR/Cas9 knockdown (Extended Data Fig. 1h-i). To further validate these
95 observations, we used Fibronectin intrabodies generated by mRNA display (FingRs) that bind to
96 endogenous PSD-95 and Gephyrin *in vivo*[20]. By expressing FingR.GFP.PSD-95 and
97 FingR.GFP.Gephyrin in OPCs, we found FingR.GFP enrichment in somas and puncta in processes
98 (Fig. 1e), similar to previous reports in neurons[20]. There were 20.3 ± 2.4 FingR.GFP.PSD-95 and
99 21.1 ± 4.0 FingR.GFP.Gephyrin puncta per OPC, which was not significantly different than IHC
100 (Fig. 1d). These results identify MAGUK/PSD-95 and Gephyrin puncta in OPCs, extending
101 previous work that reported PSD-95 in myelin sheaths[21].
102 Given that OPCs are heterogeneous according to transcriptomic and electrophysiological
103 studies[22,23], we examined the number of postsynaptic puncta across developmental stages and
104 CNS regions using IHC. We observed an increasing trend through development: both MAGUK
105 and Gephyrin puncta numbers increased from 2 dpf (14.1 ± 3.1 MAGUK; 23.6 ± 2.8 Gephyrin) to
106 14 dpf (56 ± 14.2 MAGUK; 50.9 ± 8.9 Gephyrin) (Extended Data Fig. 2a). The postsynaptic
107 puncta numbers per cell were overall similar across CNS regions, except that Gephyrin puncta
108 numbers were higher in the forebrain and midbrain (20.2 ± 1.2) compared to the spinal cord
109 (13.8 ± 0.9) (Extended Data Fig. 2b), suggesting a preference of OPCs to form synapses with
110 inhibitory neurons in the brain. Within the zebrafish spinal cord, OPC subgroups were

111 previously reported to reside in different regions (Extended Data Fig. 2c) [17]. We found that the
112 postsynaptic puncta numbers were similar between these OPC subgroups (Extended Data Fig.
113 2d).

114 **Not all MAGUK and Gephyrin puncta in OPCs are associated with other synaptic molecules**

115 Next, we tested whether these puncta align with presynaptic structures. Using the pan-
116 presynaptic marker Synapsin (Fig. 2a-f), we identified MAGUK and Gephyrin puncta in OPCs that
117 align with (Fig. 2b, e) or that do not align with (Fig. 2c, f) Synapsin in transverse sections. We
118 found similar results in sagittal sections (Extended Data Fig. 3a-b). 46.1 ± 7.4% and 38.3 ± 4.8%
119 of MAGUK and Gephyrin puncta in an OPC, respectively, align with Synapsin in the spinal cord,
120 and a similar percentage of puncta in an OPC align with Synapsin in other CNS regions (Fig. 2g).
121 To compare pre- and post-synaptic association at neuron-OPC synapses *vs*. neuron-neuron
122 synapses, we calculated colocalization ratios between Synapsin and MAGUK or Gephyrin.
123 Compared to neuron-neuron synapses (100%, normalized) from the same sections, MAGUK at
124 neuron-OPC synapses showed 103 ± 22% (2 dpf) and 70 ± 8% (14 dpf) colocalization, while
125 Gephyrin at neuron-OPC synapses showed 69 ± 10% (2 dpf) and 87 ± 5% (14 dpf) colocalization
126 (Extended Data Fig. 3c). In addition, 42.1 ± 4.8% of Gephyrin puncta in an OPC align with
127 Glycine receptors (Fig. 2h-i), and the colocalization ratio between Gephyrin and Glycine
128 receptors at neuron-OPC synapses (53.2 ± 6.6%) was less than that at neuron-neuron synapses
129 (100%, normalized) from the same sections (Extended Data Fig. 3d). These results suggest that
130 compared to neurons, more MAGUK and Gephyrin puncta in OPCs are not associated with
131 other synaptic molecules, and therefore may not represent fully functional synapses.

132 ***In vivo* imaging reveals downregulation of PSD-95-GFP and GFP-Gephyrin upon OPC**

133 **differentiation**

134 To understand synapse assembly and disassembly in OPCs, we conducted *in vivo* time-

135 lapse imaging. Due to the susceptibility of FingR.GFP to photobleaching, we generated PSD-95-

136 GFP and GFP-Gephyrin constructs (see Methods) and drove their expression with *sox10*, a pan-

137 oligodendrocyte lineage promoter. At 3 dpf in the spinal cord, we found both markers present

138 in punctate and cytosolic forms in OPCs (Fig. 3a), consistent with patterns observed in

139 neurons[24,25]. PSD-95-GFP and GFP-Gephyrin puncta size in OPCs resembled that of neurons (Fig.

140 3a-b and Extended Data Fig. 4a). There were 28.7 ± 3.9 PSD-95-GFP and 27.2 ± 3.5 GFP-

141 Gephyrin puncta per OPC (Fig. 1d), which was similar to IHC and FingR.GFP results. The slightly

142 higher PSD-95-GFP puncta number may be due to increased synaptogenesis caused by PSD-95

143 overexpression[26]. We assessed presynaptic alignment of our expression constructs *in vivo*, and

144 found that 32.8 ± 5.5% PSD-95-GFP and 43.2 ± 3.8% GFP-Gephyrin aligned with synaptophysin

145 (Extended Data Fig. 4b-c), similar to IHC. In addition, we observed an increase of PSD-95-GFP

146 and GFP-Gephyrin from 2 dpf (4.6 ± 1.1 PSD-95-GFP; 6.9 ± 1.0 GFP-Gephyrin) to 3 dpf (29.4 ±

147 4.4 PSD-95-GFP; 27.2 ± 3.5 GFP-Gephyrin) (Extended Data Fig. 4d). This increasing trend during

148 early development was comparable to IHC results (Extended Data Fig. 2a), suggesting that the

149 GFP-tagged PSD-95 and Gephyrin are regulated similarly as the endogenous proteins.

150 We wondered if postsynaptic puncta assembly and disassembly were regulated upon

151 OPC differentiation. To test this, we tracked individual OPCs over the course of their

152 development and measured the postsynaptic puncta number per cell every 20 minutes.

153 Because OPC differentiation takes several hours for all processes to either retract or transform

154 into nascent myelin sheaths, we used the disappearance of the last exploratory process as a
155 reference point. When we aligned the results from different cells, we found a decreasing trend
156 during differentiation; the postsynaptic puncta numbers reduced from 9.8 ± 2.5 PSD-95-GFP
157 and 16.5 ± 2.8 GFP-Gephyrin before the reference point to 3.9 ± 1.2 PSD-95-GFP and 9.1 ± 2.0
158 GFP-Gephyrin after the reference point (Fig. 3c-d). In cases where we observed differentiating
159 oligodendrocytes that possessed both processes and myelin sheaths, puncta were almost
160 exclusively in processes (Fig. 3e), suggesting preferential localization of synaptic puncta to
161 processes rather than nascent myelin sheaths. Altogether, these results show a downregulation
162 of postsynaptic puncta upon OPC differentiation, consistent with reduced synaptic inputs
163 reported from *ex vivo* electrophysiological studies in rodents[27,28].

164 **PSD-95-GFP and GFP-Gephyrin puncta in OPCs are dynamic and repeatedly assemble at**
165 **hotspots**

166 We next sought to analyze the dynamics of PSD-95 and Gephyrin in OPCs *in vivo* using
167 our validated expression system. The number of postsynaptic puncta per cell remained stable in
168 neurons, but fluctuated in OPCs over 30 minutes of observation (Fig. 4a and Supplementary
169 Videos 1-2). Individual puncta in neurons lasted 14,041 ± 1,187 s or about 234 min (PSD-95-GFP)
170 and 12,348 ± 3,461s or about 206 min (GFP-Gephyrin), while those in OPCs lasted only 968 ±
171 105s or about 16 min (PSD-95-GFP) and 271 ± 53s or about 5 min (GFP-Gephyrin) (Fig. 4b). 78 ±
172 4% (PSD-95-GFP) and 41 ± 12% (GFP-Gephyrin) of puncta in neurons lasted more than 10,000
173 seconds or 167 min; conversely, only 0.4 ± 0.4% (PSD-95-GFP) and 0 ± 0% (GFP-Gephyrin) of
174 puncta in OPCs did so (Fig. 4c). OPCs possess both remodeling and stable processes[17]; we found
175 puncta assembly and disassembly in both types of processes (Fig. 4f-g), suggesting that

176 postsynaptic puncta dynamics in OPCs were not simply caused by process instability. In addition,
177 we tracked GFP-Gephyrin up to 7 hours and found that puncta from the same OPC covered a
178 large space with a convex hull volume of 1.21 ± 0.21 x 10^4 μm^3, which was 50 times the volume
179 of an OPC (242 ± 28 μm^3, Fig. 4d-e). Therefore, the observed dynamic assembly enables a large
180 synaptic coverage by OPCs.

181 While postsynaptic puncta in OPCs were dynamic and covered a large space, some
182 postsynaptic puncta repeatedly assembled and disassembled in the same regions of OPC
183 processes (Fig. 4f-g). This raises the question if specific locations are preferred for synaptic
184 assembly. To test this, we plotted PSD-95-GFP and GFP-Gephyrin puncta over time and overlaid
185 heatmaps of puncta frequencies within 1 µm x 1 µm x 4 µm volumes (Fig. 4h-i). We found
186 approximately 10 such volumes where frequencies of PSD-95-GFP and GFP-gephyrin puncta
187 were 3 standard deviations higher than the average (Fig. 4j), and refer to these volumes as
188 hotspots. The Gephyrin hotspots represented only 0.3% of total synaptic space coverage of an
189 OPC (Fig. 4e). These results suggest that some postsynaptic puncta in OPCs assemble
190 repeatedly and preferentially in the confined spaces of hotspots.

191 **Gephyrin hotspots in OPCs predict future myelin sheath formation in a synaptic release-**
192 **mediated manner**

193 In zebrafish spinal cord, a myelinating oligodendrocyte forms an average of 10 myelin
194 sheaths[29], similar to the hotspot number we observed per OPC. We wondered if these hotspots
195 in OPCs were associated with future myelin sheath formation (Fig. 5a-b). To test this, we
196 measured the distances from Gephyrin hotspot centers (centroids of 1 µm x 1 µm x 4 µm
197 volumes) in an OPC to boundaries of sheaths formed after the OPC differentiated and

198 myelinated axons (Fig. 5c-d). We used the first nascent sheath appearance (time 0) to separate
199 the OPC stage and the myelinating oligodendrocyte stage. It takes up to 5 hours for an
200 oligodendrocyte to complete differentiation[29]; therefore, we identified where sheaths formed
201 approximately 6 hours after time 0 (Fig. 5c-d). In comparison, we selected 5-30 representative
202 points outside hotspots (nonhotspot) in an OPC at the beginning of imaging (see Methods) and
203 measured their distances to future myelin sheaths. The hotspot-sheath distance was
204 significantly smaller than the nonhotspot-sheath distance (Fig. 5e). Further, we examined the
205 percentage of hotspots or nonhotspots that predicted where myelin sheaths formed. We chose
206 1 µm as a threshold because we analyzed previous EM datasets of 5 dpf zebrafish[30] and found
207 an average distance of 1.4 µm between 2 myelinated axons in the dorsal spinal cord. Within 1
208 µm, 29.6 ± 8.7% of hotspots in an OPC predicted future sheath locations, while only 5.9 ± 3.4%
209 of nonhotspots did (Fig. 5f). Next, we asked if the relationship between OPC hotspots and
210 future myelin sheaths was dependent on synaptic release. We blocked synaptic release by
211 injecting tetanus toxin (TeNT) into ventricles between 2-3 dpf (Fig. 5c). We verified the TeNT
212 delivery to OPCs in the CNS with Dextran injection (see Methods). TeNT administration caused a
213 right-shift in hotspot-sheath distance distribution (Fig. 5g). The hotspot-sheath distance was not
214 significantly smaller than the nonhotspot-sheath distance with TeNT treatment (Fig. 5h). More
215 importantly, TeNT administration abolished the predication of hotspots within 1 µm (Fig. 5i).
216 This was not due to changes in OPC convex hull volume, OPC hotspot number, or myelin sheath
217 number (Extended Data Fig. 5a-c). Together, these results suggest that GFP-Gephyrin hotspots
218 are localized in proximity to future myelin sheaths and can predicate their location in a synapse-
219 release dependent manner.

220 **OPC Ca^{2+} activity is associated with synapses and predicts myelin sheath formation**

221 Given the role of Ca^{2+} signaling in sheath remodeling[18,31], we examined the relationship
222 of Ca^{2+} signaling events with synapses and sheath formation *in vivo*. With a plasma membrane-
223 targeted GCaMP6s, we analyzed OPC Ca^{2+} activity at single-cell resolution *in vivo* (Fig. 6a-b). We
224 found that 99% of Ca^{2+} events in OPCs occurred in MDs on processes, and 97% of OPCs
225 exhibited only MD Ca^{2+} activity during our recordings (Fig. 6c, Supplemental Video 3-4). We
226 examined the proximity between Ca^{2+} events in MDs and synapses, visualized by a presynaptic
227 marker, synaptophysin-TagRFP[17]. Through 3D reconstruction, we found that 34 ± 9% of MD Ca^{2+}
228 events were in <0.1 µm proximity to synaptophysin-TagRFP puncta at 5 dpf (Fig. 6d-f). We also
229 observed that Ca^{2+} events initiated from a "puncta"-like region in <0.1 µm proximity to
230 synapses (Fig. 6g-h). Next, we performed time-lapse imaging to measure the distance from MD
231 Ca^{2+} events in an OPC to sheaths formed after the OPC differentiated and myelinated axons (Fig.
232 6i-j). In comparison, we selected 5-30 representative points outside MDs (nonMD) in an OPC at
233 the beginning of imaging and measured their distances to future myelin sheaths. The MD-
234 sheath distance was significantly smaller than the nonMD-sheath distance (Fig. 6k). Next, we
235 examined the percentage of MDs that predicted where myelin sheaths formed. Within 1 µm,
236 32.0 ± 9.4% of MDs in an OPC predicted future sheath locations, while only 4.3 ± 1.2% of
237 nonhotspots did (Fig. 6l). These measurements of MD-sheath are similar to those for GFP-
238 Gephyrin hotspots and sheaths, suggesting that OPC Ca^{2+} activity *in vivo*, mainly occurring in
239 MDs, along with Gephyrin hotspots, predetermines where a subset of myelin sheaths form (Fig.
240 6m).

241 **Spontaneous synaptic release contributes to generating OPC Ca^{2+} activity *in vivo***

242 Given the close relationship between Ca^{2+} activity and synapses, we investigated the
243 role of synapses in OPC Ca^{2+} activity *in vivo.* First, we blocked synaptic release by sparsely
244 expressing tetanus toxin light chain (TeNTlc)-tdtomato[32] in axons at 5 dpf (Fig. 7a). Compared to
245 OPCs that neighbored few TeNTlc-expressing axons (< 4, few), those that neighbored many
246 TeNTlc-expressing axons (> 4, many) exhibited significantly reduced frequency of Ca^{2+} activity
247 (few 0.020 ± 0.002 vs. many 0.013 ± 0.002 Hz), peak amplitude (few 1.81 ± 0.12 vs. many 1.4 ±
248 0.08 fold), basal signal intensity (few 1.00 ± 0.10 vs. many 0.74 ± 0.06), and MD length (few 7.03
249 ± 0.38 vs. many 6.00 ± 0.25 µm) (Fig. 7b-c and Extended Data Fig. 6a). Next, we delivered
250 tetanus toxin (TeNT) to the CNS through ventricle injection at 5 dpf and analyzed Ca^{2+} activity
251 before and after injection (Fig. 7d). To ensure that TeNT (MW 150,000) was delivered
252 successfully, we coinjected Dextran (MW 3,000 or 150,000) and verified that Dextran
253 surrounded OPCs before Ca^{2+} imaging (Fig. 7e and Extended Data Fig. 6b). While control
254 solution had no effect on MD event number (before 17.0 ± 2.6 vs. after 15.5 ± 2.4) or frequency
255 of Ca^{2+} activity (before 0.0015 ± 0.0001 Hz vs. after 0.0014 ± 0.0001 Hz), TeNT administration
256 led to nearly 45% reduction in MD event number (before 25.2 ± 2.3 vs. after 14.4 ± 1.5) and
257 frequency of Ca^{2+} activity (before 0.0019 ± 0.0001 Hz vs. after 0.0010 ± 0.0001 Hz) (Fig. 7f, g,
258 Extended Data Fig. 6c and Supplementary Video 5).
259 These effects could be due to reduced neuronal activity and evoked synaptic release by
260 TeNT. To our surprise, we found that blocking neuronal action potentials with the voltage-gated
261 Na^{+} channel blocker tetrodotoxin (TTX) had no effect on the OPC Ca^{2+} activity at 5 dpf (MD
262 number per OPC: before 2.9 ± 0.6 vs. after 2.4 ± 0.5. Frequency: before 0.0014 ± 0.0002 Hz vs.
263 after 0.0012 ± 0.0002 Hz) (Fig. 7h and Extended Data Fig. 6d). We excluded the possibility of

264 ineffective TTX delivery in three ways: we observed larval paralysis within 3 minutes post-
265 injection (30/30), a complete block of motor neuron Ca^{2+} activity (Extended Data Fig. 6e-f), and
266 dextran co-injected with TTX (dextran MW3000, larger than TTX) surrounded the imaged OPCs
267 (120/120). Therefore, the reduced Ca^{2+} activity upon TeNT injection was most likely due to the
268 effects of TeNT on vesicular release at neuron-OPC synapses, rather than neuronal activity. We
269 did, however, observe reduced OPC Ca^{2+} activity upon TTX injection at the earlier timepoint of 3
270 dpf (MD number per OPC: before 3.2 ± 0.4 vs. after 2.4 ± 0.3. frequency: before 0.0014 ± 0.0001
271 Hz vs. after 0.0010 ± 0.0001 Hz), consistent with a previous report[18] and suggesting a
272 diminishing role of neuronal activity and evoked synaptic release over development. Altogether,
273 our results establish a role for spontaneous synaptic release in generating OPC Ca^{2+} activity *in*
274 *vivo*.

275 **Disruption of *nlgn3b* in OPCs impairs OPC development and myelination.**

276 Given how synaptic hotspots and Ca^{2+} activity predict myelin sheath formation, we next
277 sought to examine whether synaptic assembly was important for OPC development and
278 myelination. We targeted *neuroligin3* (*nlgn3*), which localizes to both excitatory and inhibitory
279 synapses, regulates neuronal synapse structure and function[33], and is enriched in OPCs
280 (Extended Data Fig. 1a-b)[17,19]. We developed and verified a cell-specific CRISPR/Cas9-mediated
281 gene disruption system (Extended Data Fig. 7a-e) and targeted the duplicated *nlgn3* genes
282 (*nlgn3a* and *nlgn3b*) in zebrafish. We observed a reduced oligodendrocyte percentage among
283 *nlgn3b*-targeted cells at 3 dpf and 5 dpf (Extended Data Fig. 7f-g), suggesting that loss of *nlgn3*
284 disrupts proper OPC differentiation. At 5 dpf, all labeled oligodendrocytes in control animals
285 possessed only myelin sheaths; however, 7.6 ± 1.8% of *nlgn3b*-disrupted oligodendrocytes

286 possessed both myelin sheaths and cytoplasmic processes with abnormal trapezoidal structures
287 (Fig. 8a and Extended Data Fig. 7h-i), indicating developmental defects when Nlgn3b was lost.
288 Additionally, disruption of *nlgn3b* impaired myelin sheath formation (Fig. 8b): at 3 dpf,
289 individual sheath length (ctrl 13.6 ± 0.6 µm *vs. nlgn3b* 11.4 ± 0.5 µm), sheath number (ctrl 9.9 ±
290 0.3 *vs. nlgn3b* 9.2 ± 0.3), and total length of all sheaths (ctrl 125.6 ± 4.8 µm *vs. nlgn3b* 98.0 ± 4.1
291 µm) per oligodendrocyte were reduced (Fig. 8c); at 5 dpf, sheath number (ctrl 11.2 ± 0.5 *vs.*
292 *nlgn3b* 9.1 ± 0.4) and total length of all sheaths (ctrl 368.8 ± 11.7 µm *vs. nlgn3b* 290.4 ± 10.3 µm)
293 per oligodendrocyte were reduced (Fig. 8d). Together, these results suggest a role for Nlgn3
294 specifically and synaptic assembly more broadly in oligodendrocyte differentiation and
295 myelination.
296

297 **DISCUSSION**

298 The landmark discovery of neuron-OPC synapses over 20 years ago has inspired a
299 number of studies to examine their properties with electrophysiology and EM [4], yet we still lack
300 basic understanding of their assembly and function. Here, we establish an *in vivo* model of
301 these synapses in zebrafish OPCs (Fig. 8e): they are composed of postsynaptic MAGUK (PSD-95)
302 and Gephyrin, and are developmentally regulated; they lack consistent synaptic partners and
303 exhibit dynamic synapse features; they cover large spatial volumes over time, but frequently
304 and repeatedly assemble at specific and confined "hotspots"; Gephyrin hotspots and synaptic
305 release-mediated Ca^{2+} activity predict myelination patterns; and disruption of the synaptic
306 molecule Nlgn3b impairs OPC development and myelination.

307 Previous studies suggest that neuronal activity and presynaptic release bias OL
308 myelination to "active" axons[10,12]. However, it is not clear what mechanisms mediate this
309 preference. Here, we identify a postsynaptic mechanism in OPCs that depends on presynaptic
310 release and predicts future myelination, which might partially explain how neuronal activity
311 regulates myelination. We observed approximately 30% predication rate with 1 µm threshold
312 by both GFP-Gephyrin hotspots and MD Ca^{2+} in OPCs, suggesting they may act in the same
313 pathway to determine where myelin sheaths form. One possible scenario is that presynaptic
314 release from neurons leads to synaptic activation in a nearby OPC process and subsequent Ca^{2+}
315 activity in MDs. After the OPC "senses" this neuronal location, it could enhance the synaptic
316 assembly in this location through Ca^{2+} signaling. Through such a positive-feedback mechanism,
317 "hotspots" form, while the pre- and post-synaptic interactions influence the cytoskeleton to
318 transform a process into a myelin sheath. The 30% prediction rate also reflects the likelihood of
319 other synaptic mechanisms at play, for example, PSD-95 hotspots or neuropeptides. During OPC
320 differentiation, we and others observed transient myelin sheaths that disappear rapidly after
321 formation[34]. In the future, it will be interesting to examine if hotspots and MD Ca^{2+} predict the
322 formation of transient as well as the stable sheaths. What type of presynaptic release is
323 involved in predetermining myelination patterns? Multiple neurotransmitters and
324 neuropeptides can regulate the development of oligodendrocyte lineage cells[5–8,35]. Therefore,
325 different types of neurons across CNS regions may employ one or a combination of
326 neurotransmitters and/or neuropeptides to influence myelination of their axons. Here, we
327 focus on Gephyrin-containing synapses and predict that inhibitory neurotransmitters, such as
328 glycine and GABA, may be involved in regulating the dynamic assembly and enrichment at

329 hotspots of Gephyrin. Meanwhile, how the presynaptic release sites apposed to OPC
330 postsynaptic sites are distributed in neurons is still not fully understood. A recent study
331 suggests presynaptic release sites are assembled in hotspots towards which myelin sheaths
332 grow[36]. Together with our data, this suggests that both pre- and post-synaptic sites of neuron-
333 OPC synapses are dynamically assembled at "hotspots" that predetermine where future myelin
334 sheaths form on axons.

335 Dynamic synapses lacking certain pre- or post-synaptic molecules such as PSD-95 and
336 Gephyrin puncta in OPCs have been reported in developing neurons and are considered to be
337 immature[37–40]. Therefore, many synaptic puncta in OPCs likely do not form functional and/or
338 mature synapses. These synapse features are in tune with an OPC's dynamic cell biological
339 properties in which proliferation, migration, and process remodeling must be coordinated
340 before myelination. Interestingly, transcripts and/or proteins of synaptic genes are detected
341 even after OPCs differentiate and myelinate axons, although often at reduced levels[17,19,21,22]. It
342 is possible that the synaptic machinery and mechanisms we identify in OPCs also play a role in
343 sheath elongation and shortening. The dynamically assembled postsynaptic components in
344 OPCs cover a rather large space compared to the volume of an OPC alone, allowing these cells
345 to effectively survey their environments. Our observation that synaptic puncta numbers reduce
346 upon OPC differentiation provides a structural basis for the previously reported reduced
347 synaptic functions during this transition[27,28]. These data, together our observations that
348 synaptic puncta in OPCs increase during early development, suggest that synaptic assembly in
349 OPCs is finely regulated by development.

350 Several studies have identified synaptic mechanisms underlying Ca^{2+} elevation in OPCs
351 under conditions of increased neuronal activity (*e.g.*, through axon stimulation) with a focus on
352 somal activity[14–16,41]. We find that OPC Ca^{2+} activity *in vivo* mainly occurs in MDs and requires
353 spontaneous synaptic release. Neuronal activity and evoked synaptic release play a role in OPC
354 Ca^{2+} activity at 3 dpf, but to our surprise not at 5 dpf. Considering that OPC differentiation
355 initiates at 3 dpf, this suggests that OPCs are sensitive to neuronal activity through Ca^{2+}
356 signaling at this critical stage of development. This sensitivity may be important for OPC
357 differentiation and myelination. In our Ca^{2+} assays, we observe "outlier" OPCs that behave
358 differently from the majority of OPCs. For example, some OPCs exhibit no change or even an
359 increase of Ca^{2+} activity upon TeNT treatment while most OPCs exhibit reduction; some OPCs
360 exhibit reduced Ca^{2+} activity while others exhibit no change of or increased Ca^{2+} activity upon
361 TTX treatment at 5 dpf. These "outlier" OPCs and activity could be due to Ca^{2+} generated from
362 synapse-independent mechanisms, such as ER-mediated Ca^{2+} release. In line with this, nearly 61%
363 of Ca^{2+} MDs do not associate with presynaptic markers, and nearly 55% residual Ca^{2+} activity
364 remains after TeNT treatment, suggesting synapse-independent Ca^{2+}-inducing mechanisms in
365 OPCs. Overall, we find that OPC Ca^{2+} activity *in vivo* is complex and might be mediated by
366 different mechanisms than OPCs in *ex vivo* assays. While previous studies used axonal
367 stimulation to study neuronal activity-induced OPC Ca^{2+} response, our study of *in vivo* OPC Ca^{2+}
368 activity reveals that neuronal activity does not contribute to Ca^{2+} activity at certain
369 developmental stages. This suggests that axon stimulation may drive extrinsic Ca^{2+} activity that
370 otherwise would not naturally occur, cautioning the usage of axon stimulation to study OPC
371 Ca^{2+} activity.

372 Nlgn3's function is best understood at synapses. Our finding that *nlgn3b* knockdown in
373 oligodendrocyte lineage cells impairs OPC differentiation and myelination suggests a potential
374 role of synapses in OPCs. This is consistent with our observations that GFP-Gephyrin hotspots
375 and Ca^{2+} MDs in OPCs predict where myelin sheaths form in oligodendrocytes. Given Nlgn3's
376 broad presence and function at both Glutamatergic, GABAergic and Glycinergic synapses, we
377 expected that this approach has a larger impact on OPC activity and influences more OPCs than
378 disruption of single synaptic receptors. In line with our findings, an *in vitro* study found that
379 incubating neuron-glia co-cultures with extracellular domains of Nlgn3 inhibits OPC
380 differentiation and axon wrapping[42]. However, we can't rule out a non-synaptic function of
381 Nlgn3 that could contribute to these phenotypes. In astrocytes, *Nlgn3*'s knockdown reduced
382 astrocyte neuropil infiltration volumes[43]. Because astrocytes do not form synapses with
383 neurons, this study suggests a non-synaptic role of Nlgn3 in astrocytes. Whether Nlgn3 plays a
384 non-synaptic role in OPCs and oligodendrocytes remains to be understood.

385 The signaling pathways downstream of synapse/Ca^{2+} MDs in OPCs also remain to be
386 elucidated. Local Ca^{2+} activity might alter the cytoskeleton via Ca^{2+}-dependent kinases [44] or
387 affect lipid raft domains to change local signaling[41]. Notably, focal adhesion kinases (FAKs) can
388 affect cell motility and interactions with other cells and are tightly connected to Ca^{2+} activity[45].
389 FAKs promotes glioma growth downstream of Nlgn3 in response to neuronal activity[3,46], and we
390 find that that *nlgn3* knockdown leads to impaired OPC differentiation and oligodendrocyte
391 myelination. Therefore, Nlgn3 and FAKs may act downstream of synapses and Ca^{2+} signaling to
392 regulate OPC behavior during development as well as glioma growth. Overall, our *in vivo* study
393 establishes a relationship between neuronal activity, synaptic assembly, and Ca^{2+} activity at

394 neuron-OPC synapses, and reveals their roles in predicting where myelin sheaths form in
395 oligodendrocytes. This model inspires future directions to further investigate the pre- and post-
396 synaptic mechanisms underlying neuron-OPC interactions that regulate OPC development and
397 shape myelination.
398

399 ## ACKNOWLEDGMENTS

400 This work was supported by NMSS postdoctoral fellowship FG-1907-34613 (JL), Warren Alpert
401 Distinguished Scholar Award (JL), and NIH/NINDS grant 1R21NS120650 (KRM). We thank
402 Dwight Bergles, Anusha Mishra, Alex Nechiporuk, and members of the Monk lab for discussions
403 and critical reading of the manuscript. We are indebted to Austin Forbes, Tia Perry, and Grace
404 Halsell-Vore for fish care. We thank Rafael Almeida, Paul Brehm, Marc Freeman, Henrique von
405 Gersdorff, Eric Gouaux, David Lyons, Lei Ma, and Teresa Nicolson for reagents and suggestions
406 as well as Fernanda Coelho, Stefanie Kaech Petrie, and the OHSU microscopy core staff for
407 feedback and assistance in imaging. We thank Lori Vaskalis for graphic design.
408

409 ## AUTHOR CONTRIBUTIONS

410 J.L. and K.R.M. conceived the project. J.L. carried out experiments and data analyses. T.M.
411 generated constructs for *nlgn3a* and *nlg3b* disruption. T.C. provided key resources prior to their
412 publication. J.L. and K.R.M wrote the manuscript, and all authors edited the manuscript.
413

414 ## DECLARATION OF INTERESTS

415 The authors declare no competing interests.

416

417 **Additional information**

418 **Supplementary Information** is available for this paper.

419 **Correspondence and requests for materials** should be addressed to Jiaxing Li or Kelly Monk.

420

421

422 FIGURE TITLES AND LEGENDS

423 **Fig. 1. Postsynaptic organizers MAGUK/PSD-95 and Gephyrin are present in zebrafish spinal cord OPCs**
424 (a) Top, schematic fish model showing transverse section orientation; bottom, distribution of soma and
425 axons & synapses in spinal cord transverse sections.
426 (b-c) Representative IHC images of (b) MAGUK and (c) Gephyrin in *Tg(olig1:Kalta4,10xUAS:myrGFP)*
427 spinal cord at 3 dpf. From left, spinal cord sections, enlarged regions, and 3D-reconstructed images. In
428 3D-reconstructed images, only the postsynaptic puncta that fall within OPC process volume are shown
429 (magenta sphere).
430 (d) Quantification of puncta number per OPC by IHC (MAGUK and Gephyrin), FingR.GFP (PSD-95 and
431 Gephyrin), and GFP-tagged (PSD-95 and Gephyrin) in the spinal cord. From left, n = 20, 32, 18, 24, 15,
432 and 14 cells from at least 10 fish; F[69] = 3.937, F[52] = 1.381.
433 (e) Representative images and enlarged regions of FingR.GFP.PSD-95 and FingR.GFP.Gephyrin driven by
434 *olig1* promoter in OPCs. OPC somas are indicated with arrows.
435 All data are represented as mean ± SEM; (d) one-way ANOVA followed by Tukey's test; scale bars 5 μm.
436

437 **Fig. 2. Not all MAGUK and Gephyrin puncta in OPCs are associated with other synaptic components**
438 (a-f) Representative transverse IHC images of (a-c) MAGUK and (d-f) Gephyrin with Synapsin in
439 *Tg(olig1:Kalta4,10xUAS:myrGFP)* spinal cord OPCs at 3 dpf. (a and d) Spinal cord sections; (b, c, e, f)
440 enlarged regions with 3D reconstruction (left) and Synapsin alignment (right). The postsynaptic puncta
441 that fall within OPC process volumes are shown in 3D-reconstructed images (green sphere) and are
442 indicated with arrowheads in Synapsin alignment images. Postsynaptic puncta either align (b and e) with
443 Synapsin or do not (c and f).
444 (g) The % of MAGUK and gephyrin puncta in an OPC that align with presynaptic Synapsin in different CNS
445 regions at 3 dpf. From left, n= 32, 57, 38, 33, 16 and 39 cells from at least 10 fish; F[214] = 3.5240.
446 (h) Representative IHC images of Gephyrin and Glycine receptors (GlyR) in
447 *Tg(olig1:Kalta4,10xUAS:myrGFP)* spinal cord OPCs at 3 dpf. OPC boundaries are indicated in green.
448 Gephyrin puncta either align with GlyR (green arrowheads) or do not (magenta arrowheads).
449 (i) The % of Gephyrin puncta in an OPC that align with GlyR in spinal cord at 3 dpf. n = 12 cells from 7 fish.
450 All data are represented as mean ± SEM; N.S., not significant; (g) one-way ANOVA followed by Tukey's
451 test; Scale bars 5 μm.
452

453 **Fig. 3. *In vivo* imaging reveals downregulation of PSD-95-GFP and GFP-Gephyrin upon OPC**
454 **differentiation**

455 (a-b) Representative images of PSD-95-GFP and GFP-Gephyrin (magenta) in spinal cord (a) OPCs and (b)
456 neurons at 3 dpf. Cell membranes indicated with cyan.
457 (c-d) Quantification of (c) PSD-95-GFP and (d) GFP-Gephyrin puncta number in OPCs before and after the
458 last process disappearance, set as time zero, during differentiation. Left, individual traces (grey lines)
459 with the average (black line) and the standard deviation (shade). Right, paired comparison before and
460 after time zero. (c) n= 12 cells from 8 fish; t[11] = 3.922. (d) n= 12 cells from 8 fish; t[11] = 2.705.
461 (e) Representative images of PSD-95-GFP and GFP-Gephyrin (magenta) in differentiating
462 oligodendrocytes (cyan) at 2-3 dpf. Nascent sheaths are indicated with black arrowheads, and processes
463 are indicated with magenta arrowheads.
464 All data are represented as mean ± SEM; N.S., not significant; (c-d) ratio-paired *t*-test; scale bars 5 µm.
465
466 **Fig. 4. PSD-95-GFP and GFP-Gephyrin puncta in OPCs are dynamic and repeatedly assemble at**
467 **hotspots**
468 (a) Normalized puncta number per cell of PSD-95-GFP and GFP-Gephyrin in neurons and OPCs within 30
469 minutes. Black line, average; shaded area, standard deviation. From left, n = 12, 3, 4, and 6 cells from 6,
470 10, 4, and 4 fish.
471 (b-c) Quantification of PSD-95-GFP (green) and GFP-Gephyrin (magenta) puncta duration in (b) log scale
472 and (c) % of stable puncta that lasts over 10,000 seconds in neurons and OPCs at 3 dpf. (b) n = 13 and 3
473 cells from 6 and 3 fish; t[14] = 5.152 and t[9] = 4.82. (c) n = 5 and 7 cells from 4 and 4 fish; t[14] = 9.989
474 and t[10] = 4.159.
475 (d) Convex hull of GFP-Gephyrin puncta in an OPC over 7 hours. The OPC membrane in the beginning of
476 imaging is shown in magenta.
477 (e) Quantification of convex hull volume of GFP-Gephyrin from (d), OPC volume and volume of GFP-
478 Gephyrin hotspot space in an OPC. From left, n= 11, 23, and 18 cells from at least 10 fish; t[39] = 6.561
479 and t[32] = 8.480.
480 (f-g) Representative time-lapse images of (f) PSD-95-GFP and (g) GFP-Gephyrin within OPC processes.
481 The numbers indicate the corresponding puncta in h and i. Puncta #1 and #3 are in stable processes;
482 puncta #2 and #4 are in dynamic processes. The dashed lines outline the process, and arrowheads
483 indicate puncta appearance. Time unit is in minutes.
484 (h-i) Heatmaps of puncta appearance frequency over time for (h) PSD-95-GFP and (i) GFP-Gephyrin. 30%
485 of max frequency is used as coloring threshold: below threshold, grey; above threshold, a shade of
486 magenta corresponding to the frequency. Loci with high puncta appearance frequency (> 3 standard
487 deviations above average) are marked with arrowheads. The numbers with green arrowheads indicate
488 puncta shown in time lapse images in Fig. 4f-g. Bottom left, images of OPCs with puncta marked with
489 magenta circles.
490 (j) Quantification of loci with high puncta appearance frequency in OPCs. From left, n = 3 and 7 cells
491 from 3 and 5 fish.
492 All data are represented as mean ± SEM; (b, c, and e) unpaired *t*-test; Scale bars, 5 µm.
493
494 **Fig. 5. Gephyrin hotspots predict future myelin sheath formation in a synaptic release-mediated**
495 **manner**
496 (a-b) Representative images of GFP-Gephyrin (green) in an oligodendrocyte lineage cell (magenta) at 2
497 different stages: (a) OPC stage that is 8 hours prior to myelination and (b) oligodendrocyte stage that is 6
498 hours after myelination begins.
499 (c) Schematic showing the imaging protocol of individual OPCs that differentiate into myelinating
500 oligodendrocytes. The first sheath appearance is designated as time 0. Images from up to 10 hours to 1
501 hour before time 0 are used to identify OPC hotspots, and images around 6 hours after time 0 are used
502 to define sheath regions. TeNT is delivered through ventricle injection before imaging.

503 (d) Single-plane merged image of Gephyrin puncta frequency heatmap at OPC stage and sheath regions
504 at oligodendrocyte stage. Hotspots (magenta), hotspot centers (green), and sheaths (yellow) are
505 indicated. Hotspots that existed within where myelin sheaths form are indicated with arrowheads.
506 (e) Quantification of hotspot-sheath and nonhotspot-sheath distances. n = 8 cells from 7 fish.
507 (f) Percentage of hotspots or nonhotspots that predict where myelin sheaths form within 1 µm in an
508 OPC. n = 8 cells from 7 fish.
509 (g) Frequency distribution of hotspot-sheath distances in control- and TeNT-treated OPCs. F[13, 168] =
510 11.39.
511 (h) Quantification of hotspot-sheath and nonhotspot-sheath distances with TeNT treatment. n = 6 cells
512 from 6 fish.
513 (i) Percentage of hotspots or nonhotspots that predict where myelin sheaths form within 1 µm in an
514 OPC with TeNT treatment. n = 6 cells from 6 fish.
515 (e,f,h,i) Wilcoxon matched-pairs signed rank test; (g) Two-way ANOVA and Fisher's LSD test; scale bars 5
516 µm.
517
518 **Fig. 6. OPC Ca^{2+} activity is associated with synapses and predicts myelin sheath formation**
519 (a) Representative images of plasma membrane-targeted myrGCaMP6s in an OPC (grey) showing activity
520 in MDs (cyan).
521 (b) Individual traces plotting myrGCaMP6s intensity ($\Delta F/F_{average}$) in 5 MDs from Fig. 6A. Scale bar, 100%
522 and 50s.
523 (c) Left, the occurrences of Ca^{2+} activity in MDs vs. soma; right, the number of OPCs with only MD
524 activity vs. OPCs with both MD and somal activity. n = 180 cells from 107 fish.
525 (d) Representative images of a Ca^{2+} MD (cyan) in an OPC and presynaptic synaptophysin-tagRFP
526 (magenta).
527 (e) 3-D reconstruction from (d) showing synaptophysin-tagRFP puncta (magenta) that are within 0.1 µm
528 from the OPC surface (arrowheads).
529 (f) The percentage of Ca^{2+} MDs that are associated with synaptophysin-tagRFP. n = 7 cells from 7 fish.
530 (g) Two Ca^{2+} spikes initiate as puncta and then spread to form MDs, indicated by blue arrowheads. The
531 time is in seconds.
532 (h) The two MDs from (g) initiate in proximity (within 0.1 µm) to presynaptic synaptophysin-tagRFP
533 (magenta), indicated by white arrowheads.
534 (i) Ca^{2+} imaging protocol of individual OPCs that differentiate into oligodendrocytes. The first sheath
535 appearance is designated as time 0. Images up to 6 hours before time 0 are used to identify OPC Ca^{2+}
536 events in MDs, and images around 6 hours after time 0 are used to define sheath regions.
537 (j) Merged single-plane image of Ca^{2+} MDs at OPC stage and sheath regions at oligodendrocyte stage.
538 Ca^{2+} MDs (blue) and sheaths (yellow) are indicated.
539 (k) Quantification of MD-sheath and nonMD-sheath distances. n = 9 cells from 7 fish.
540 (l) Percentage of MDs or nonMDs that predict where myelin sheaths form within 1 µm in an OPC. n = 9
541 cells from 7 fish.
542 (m) Schematic showing GFP-Gephyrin hotspots and MDs in OPCs similarly predict where myelin sheaths
543 form in oligodendrocytes.
544 (k and l) Wilcoxon matched-pairs signed rank test; scale bars 5 µm.
545
546 **Fig. 7. Spontaneous synaptic release contributes to generating OPC Ca^{2+} activity *in vivo***
547 (a) Schematic showing OPCs neighboring few or many TeNTlc-expressing axons in our sparse-labeling
548 approach.
549 (b) Representative images of OPCs neighboring few (<4) and many (≥4) axons expressing TeNTlc-
550 tdtomato.

551 (c) The frequency of Ca^{2+} activity and peak amplitude in OPCs that neighbor few (<4) and many (≥4)
552 TeNTlc-expressing axons at 5 dpf. Few, n = 14 cells from 8 fish; many, n = 26 cells from 15 fish; t[37] =
553 2.420 and t[38] = 2.958.
554 (d) Experimental paradigm of reagent delivery and Ca^{2+} imaging.
555 (e) Representative single-plane images of individual spinal cord OPCs immediately and 10 min after
556 ventricle injection of Dextran^{3000} Texas Red (magenta) in *Tg(olig1:Kalta4,10xUAS:myrGFP)* animals.
557 (f) Representative images of myrGCaMP6s (grey) and Ca^{2+} MDs (cyan) in control and TeNT treatment
558 condition.
559 (g) Ca^{2+} MD number and frequency of Ca^{2+} activity per MD in OPCs before (blue) and after (magenta)
560 injection of control or TeNT solution at 5 dpf. Paired data are indicated with grey lines. Control, n = 17
561 from 13 fish; TeNT, n = 26 cells from 18 fish; from left, t[16] = 1.303, t[512] = 0.5899, t[25] = 6.189 and
562 t[959] = 8.853.
563 (h) Ca^{2+} MD number and frequency of Ca^{2+} activity per MDs in OPCs before (blue) and after (magenta)
564 injection of control or TTX solution at 3 dpf and 5 dpf. Paired data are indicated with grey lines. From left,
565 n = 15 ,31, 13, and 17 cells from 7, 13, 6, and 9 fish; t[14] = 1.000, t[30] = 2.2010, t[12] = 0.1125, t[16] =
566 0.8552, t[66] = 0.6158, t[163] = 2.3440, t[81] = 0.5877 and t[89] = 0.5379.
567 All data are represented as mean ± SEM; N.S., not significant; (c) unpaired *t*-test or (g-h) paired *t*-test;
568 scale bars 5 µm.
569
570 **Fig. 8. Disruption of *nlgn3b* in OPCs impairs development and myelination.**
571 (a) Morphology of oligodendrocytes with control- (ctrl) and *nlgn3b*-targeted for cell-specific knockdown
572 at 5 dpf. Top, 3D-reconstructed single oligodendrocyte with sheath (colored) and non-sheath (gray).
573 Bottom, single plane with sheath (black arrowheads) and processes (magenta arrowheads).
574 (b) Representative images of myelin sheaths from oligodendrocytes with control- (ctrl) and *nlgn3b*-
575 targeted for cell-specific knockdown at 3 and 5 dpf.
576 (c-d) Quantification of myelin sheath average lengths, number, and total length per oligodendrocyte
577 from (b) at 3 dpf (c) and 5 dpf (d) in ctrl-, *nlgn3a*-, and *nlgn3b*-targeted fish. (c) n = 121, 30, and 170 cells
578 from 78, 26, and 97 fish. (d) n = 118, 80, and 152 cells from 80, 61, and 93 fish.
579 (e) *In vivo* model of neuron-OPC synapses: they are composed of MAGUK and Gephyrin and contribute
580 to OPC Ca^{2+} activity through spontaneous release; they exhibit immature features: lack of synaptic
581 components and fast assembly, which enable OPCs to survey large spatial volumes; synaptic assembly
582 hotspots and associated Ca^{2+} activity at the OPC stage predict where a subset of myelin sheaths form at
583 the oligodendrocyte stage; synaptic assembly is regulated through development while disruption of the
584 synaptic molecule *nlgn3b* impairs OPC development and myelination.
585 All data are represented as mean ± SEM; N.S., not significant; (c-d) Kruskal-Wallis test followed by
586 Dunn's multiple comparisons test; scale bar 5 µm.
587

588

589 **EXTENDED DATA FIGURE TITLES AND LEGENDS**

590 **Extended Data Fig. 1. MAGUK/PSD-95, Gephyrin, and Nlgn3 are present in OPCs, related to Fig. 1**
591 (a) RNA-seq expression of murine *Dlg4* (*PSD-95*), *Gephyrin*, and *Nlgn3* in different CNS cell types[19].
592 Microglia and Macrophage (Micro/Macro); Newly formed oligodendrocyte (NFO); Myelinating
593 oligodendrocyte (MOL).

594 (b) Single cell RNA-seq expression of zebrafish *dlg4* (*a*/*b*), *gephyrin* (*a*/*b*), and *nlgn3* (*a*/*b*)[17]. Vascular
595 lepotomeningeal cell (VLMC); Myelinating oligodendrocyte (MOL).
596 (c) Representative IHC images of PSD-95 in *Tg(olig1:Kalta4,10xUAS:myrGFP)* spinal cord at 3 dpf. From
597 left, spinal cord sections, enlarged regions, and 3D-reconstructed images to reveal OPC surface and
598 postsynaptic puncta within OPC processes (magenta sphere).
599 (d) Schematic fish model showing sagittal planes.
600 (E-F) Two representative single-sagittal-plane IHC images showing (e) MAGUK and (f) Gephyrin within
601 OPCs in *Tg(sox10:GFP-caax)* spinal cord at 3 dpf. OPCs identified by GFP and shown in cyan. Arrowheads
602 indicate synaptic puncta. The colors are inverted to optimize visualization.
603 (g) % of puncta localized to OPC soma and process. MAGUK, n = 18 cells from 8 fish; Gephyrin, n = 40
604 cells from 15 fish.
605 (h) IHC images of Gephyrin in the 5 dpf spinal cord in wild-type and F0 larvae with *gephyrin* knocked
606 down by sgRNA targeting *gephyrina*^{ex2} and *gephyrinb*^{ex7} and Cas9 protein.
607 (i) Quantification of Gephyrin intensity in (h). n = 5 and 9 fish for each group; t[12] = 7.322.
608 All data are represented as mean ± SEM; (i) unpaired *t*-test; scale bars 5 μm.
609
610 **Extended Data Fig. 2. MAGUK and Gephyrin puncta numbers in OPCs increase during early**
611 **development and exhibit small differences across CNS regions, related to Fig. 1**
612 (a) Quantification of MAGUK (green) and Gephyrin (magenta) puncta number per cell in the spinal cord
613 at different ages by IHC. From left, n = 10, 8, 8, 8, 7, 8, 8, and 7 cells from at least 6 fish; t[33] = 5.730
614 and t[30] = 7.040.
615 (b) Quantification of MAGUK (green) and Gephyrin (magenta) puncta number per OPC at 3 dpf across
616 different CNS regions. From left, n = 34, 59, 43, 34, 18, and 40 cells from at least 10 fish; F[227] = 13.10.
617 (c) Schematic model showing the neuron-rich (NR) and axon & synapse-rich (AR) regions and two
618 representative images showing OPCs with soma localized to NR (top) and AR (bottom) regions in
619 *Tg(olig1:Kalta4,10xUAS:myrGFP)* spinal cord.
620 (d) Quantification of MAGUK (green) and Gephyrin (magenta) puncta number per cell in OPCs localized
621 to NR or AR regions at 2-3 dpf. From left, n = 14, 5, 15 and 10 cells from at least 5 fish; t[17] = 0.3372 and
622 t[23] = 0.8770.
623 All data are represented as mean ± SEM; N.S., not significant; (a-b) one-way ANOVA followed by Tukey's
624 test and (d) unpaired *t*-test; scale bar 5 μm.
625
626 **Extended Data Fig. 3. More MAGUK and Gephyrin puncta in OPCs are not associated with other**
627 **synaptic molecules compared to neurons, related to Fig. 2**
628 (a-b) Representative single-sagittal-plane IHC images of (a) MAGUK and (b) Gephyrin with presynaptic
629 marker Synapsin in *Tg(sox10:GFP-caax)* spinal cord at 3 dpf. From left, merged channels, MAGUK or
630 Gephyrin channel, and Synapsin channel. Black arrowheads indicate the postsynaptic puncta in OPCs
631 that align with presynaptic Synapsin. Magenta arrowheads indicate the postsynaptic puncta in OPCs that
632 do not align with presynaptic Synapsin.
633 (c) Colocalization ratio of MAGUK (green) or Gephyrin (magenta) in OPCs with Synapsin, normalized to
634 neurons at 2 dpf and 14 dpf. From left, n = 9, 7, 9, and 7 OPCs from at least 5 fish; t[8] = 0.1426, t[6] =
635 3.6380, t[8] = 3.2880, t[6] = 2.5400.
636 (d) Colocalization ratio of Gephyrin with GlyR in OPCs, normalized to neurons at 3 dpf. n = 11 cells from
637 7 fish; t[10] = 7.049.
638 All data are represented as mean ± SEM; N.S., not significant; (c-d) paired *t*-test; Scale bars 5 μm.
639
640 **Extended Data Fig. 4. *In vivo* characterization of PSD-95-GFP and GFP-gephyrin, related to Fig. 3**

641 (a) Puncta diameter of PSD-95-GFP (green) and GFP-Gephyrin (magenta) in neurons and OPCs at 2-3 dpf
642 in the spinal cord. From left, n = 10, 11, 15, and 29 cells from at least 8 fish; t[19] = 1.8200 and t[42] =
643 0.2447.
644 (b) Representative images of PSD-95-GFP or GFP-Gephyrin (green) and synaptophysin-TagRFP (magenta)
645 in spinal cord OPCs at 3 dpf. From left, single plane images, enlarged regions, and Imaris "Spot"-
646 processing to reveal pre- (magenta sphere) and post- (green sphere) synaptic puncta.
647 (c) The % of PSD-95-GFP and GFP-gephyrin puncta in an OPC that align with presynaptic synaptophysin-
648 TagRFP in the spinal cord in (b). n = 13 and 20 cells from at least 10 fish.
649 (d) Quantification of PSD-95-GFP (green) and GFP-Gephyrin (magenta) puncta number per cell in the
650 spinal cord at 2 dpf and 3 dpf. From left, n = 16, 18, 29, and 14 cells from at least 5 fish; t[32] = 5.238 and
651 t[41] = 7.147.
652 All data are represented as mean ± SEM; (a, d) unpaired *t*-test. Scale bars 5 µm.
653
654 **Extended Data Fig. 5. Gephyrin hotspots predict myelin sheath formation in a synaptic release-**
655 **mediated manner, related to Fig. 5**
656 (a-c) Quantification of (a) convex hull volume, (b) hotspot number, and (c) sheath number in control and
657 TeNT treatment conditions. (a) n = 11 and 6 cells from 10 and 6 fish; (b) n = 18 and 6 cells from 16 and 6
658 fish; (c) n = 11 and 6 cells from 10 and 6 fish.
659 All data are represented as mean ± SEM; (a-c) Mann-Whitney test.
660
661 **Extended Data Fig. 6. The role of synaptic release and neuronal activity in generating OPC Ca^{2+} activity,**
662 **related to Fig. 7**
663 (a) Basal GCaMP6s intensity and MD feret's diameter in OPCs that neighbor few (< 4) and many (≥ 4)
664 TeTxLc-expressing axons at 5 dpf. Few, n = 14 cells from 8 fish; many, n= 26 cells from 15 fish; t[38] =
665 2.375 and t[38] = 2.351.
666 (b) Representative image of individual spinal cord OPCs 50 min after ventricle injection of $Dextran^{150,000}$
667 Antonia Red (magenta) in *Tg(olig1:Kalta4,10xUAS:myrGcamp6s)* fish.
668 (c) Quantification of peak amplitude, peak duration, area of Ca^{2+} MD, frequency of Ca^{2+} activity per cell,
669 basal intensity, and MD Feret's diameter in OPCs before (blue) and after (magenta) injection of control
670 or TeNT solution at 5 dpf. Paired data are indicated with grey lines. Control, n = 17 cells from 13 fish;
671 TeNT, n = 26 cells from 18 fish; from left, t[16] = 0.4575, t[25] = 1.158, t[16] = 0.3358, t[25] = 2.312, t[16]
672 = 1.159, t[25] = 1.872, t[16] = 0.5831, t[25] = 5.077, t[16] = 1.039, t[27] = 4.028, t[16] = 1.434, and t[29] =
673 1.421.
674 (d) Quantification of Ca^{2+} MD number and frequency of Ca^{2+} activity per MD in OPCs before (blue) and
675 after (magenta) injection of control or TTX solution at 3 dpf and 5 dpf. Paired data are indicated with
676 grey lines. From left, n = 15 ,31, 13, and 17 cells from 7, 13, 6, and 9 fish; t[9] = 1.3490, t[23] = 2.2340,
677 t[9] = 0.7957, t[10] = 1.0540, t[9] = 0.4645, t[23] = 0.8590, t[9] = 0.8009, t[10] = 0.2402, t[9] = 0.4605,
678 t[23] = 0.7737, t[9] = 0.2900 and t[10] = 0.2361.
679 (e) Representative images of a primary motor neuron visualized by injecting *mnx1:gal4* into
680 *Tg(10xUAS:myrGCaMP6s).*
681 (f) Frequency of Ca^{2+} activity per cell before (blue) and after (magenta) injection of control or TTX
682 solution in motor neurons at 5 dpf. n = 7 and 6 cells from 5 and 5 fish; t[6] = 1.6220 and t[5] = 3.7970.
683 All data are represented as mean ± SEM; N.S., not significant; (a) unpaired *t*-test or (c-d, f) paired *t*-test;
684 scale bars 5 µm.
685
686 **Extended Data Fig. 7. Disruption of *nlgn3b* in OPCs impairs OPC development and myelination, related**
687 **to Fig. 8**

688 (a) Schematic of Tol2 plasmid (10xUAS:myrmScarletI-p2A-Cas9, U6:sgRNA1;U6:sgRNA2) constructed and
689 used to induce cell-specific Cas9 expression with membrane labeling and 2 separate U6-driven sgRNAs.
690 (b) Representative gel images of digested PCR product of genomic regions targeted by the sgRNAs. Each
691 lane represents a single embryo at 1 dpf. The left 4 lanes are uninjected (-) and the right 4 lanes are
692 injected (+) with sgRNAs and Cas9 protein.
693 (c) Schematic of larva with sparsely labeled oligodendrocyte lineage cells resulting from *Tg(sox10:Kalta4)*
694 crossed with transgenic fish carrying the plasmid from (a).
695 (d) Representative images of single oligodendrocytes in the spinal cord of *Tg(10xUAS:myrmScarletI-p2A-*
696 *Cas9, U6:ctrl-sgRNA1;U6:ctrl-sgRNA2)* and *Tg(10xUAS:myrmScarletI-p2A-Cas9, U6:myrf*^{ex3}-
697 *sgRNA;U6:myrf*^{ex4}*-sgRNA)* at 6 dpf. Knockdown of Myrf serves as a control for our targeting approach.
698 (e) Quantification of myelin sheath length in (d). n = 24 and 22 cells from 15 fish; t[44] = 2.247.
699 (f) Representative images of an OPC and an oligodendrocyte.
700 (g) Percentage of oligodendrocytes (in contrast to OPCs) in ctrl-, *nlgn3a*-, and *nlgn3b*-targeted fish at 3
701 dpf and 5 dpf. 3 dpf, n = 144, 82, and 152 cells from 78, 26, and 97 fish, F[6] = 15.90; 5 dpf, n = 119, 84,
702 and 170 cells from 80, 61, and 93 fish, F[6] = 7.343.
703 (h) Percentage of oligodendrocytes that possess both myelin sheath and abnormal processes in ctrl-,
704 *nlgn3a*-, and *nlgn3b*-targeted fish at 5 dpf. n = 119, 84, and 170 cells from 80, 61, and 93 fish, F[6] =
705 13.52.
706 (i) 4 single planes of a trapezoid-shaped process in an oligodendrocyte in *nlgn3b*-targeted larvae at 5 dpf.
707 Myelin sheaths are indicated by black arrowheads and abnormal processes by magenta arrowheads.
708 All data are represented as mean ± SEM; N.S., not significant; (e) unpaired *t*-test and (g,h) one-way
709 ANOVA followed by Tukey's test; scale bars 5 μm.
710
711 **SUPPLEMENTARY VIDEOS WITH TITLES AND LEGENDS**

712 ***Video 1. Time-lapse images of GFP-Gephyrin in an OPC***
713 Representative video of sox10:myrTagRFP-T-P2A-GFP-Gephyrin in an OPC that eventually differentiates
714 in the spinal cord of a 3 dpf larva.
715
716 ***Video 2. Time-lapse images of GFP-Gephyrin in a neuron***
717 Representative video of 10xUAS:GFP-Gephyrin in a neuron in the spinal cord of a *Tg(sox10:Kalta4)* larva
718 at 3 dpf.
719
720 ***Video 3. Time-lapse images of myrGCaMP6s in an OPC***
721 Representative video of Ca^{2+} activity in an OPC in a *Tg(olig1:Kalta4,10xUAS:myrGCaMP6s)* larva at 5 dpf.
722
723 ***Video 4. Time-lapse images of myrGCaMP6s in an OPC with both MD and somal Ca^{2+} activity***
724 Video of Ca^{2+} activity in an OPC with multiple events including a somal event in a
725 *Tg(olig1:Kalta4,10xUAS:myrGCaMP6s)* larva at 5 dpf.
726
727 ***Video 5. Time-lapse images of myrGCaMP6s in an OPC before and after injection of TeNT at 5 dpf***
728 Representative 10-minute video of Ca^{2+} activity in an OPC before (left) and after (right) injection of TeNT
729 in a *Tg(olig1:Kalta4,10xUAS:myrGCaMP6s)* larva at 5 dpf.
730
731 **SUPPLEMENTARY TABLES WITH TITLES AND LEGENDS**

732 ***Table 1. A list of primers used in this study***

733 Related to STARS Methods.
734

735 # METHODS

736 ## RESOURCE AVAILABILITY

737 ### Lead contact

738 Further information and requests for resources and reagents should be directed to and will be
739 fulfilled by the lead contacts, Jiaxing Li (lijia@ohsu.edu) or Kelly Monk (monk@ohsu.edu).

740 ### Materials availability

741 All reagents generated in this paper will be shared by the lead contacts upon request.

742 ### Data and code availability

743 All data reported in this paper will be shared by the lead contacts upon request.
744 All original code is available from the lead contacts upon request.
745 Any additional information required to reanalyze the data reported in this paper is available
746 from the lead contacts upon request.
747

748 ## EXPERIMENTAL MODEL AND SUBJECT DETAILS

749 We used the following existing zebrafish lines and strains: *Tg(sox10:Kalta4)*[47], *Tg(olig1:Kalta4)*[17],
750 *Tg(huc:synaptophysin-tagRFP)*[17], *Tg(olig2:dsRed)*, *Tg(sox10:GFP-caax)*, *nacre*, and AB. The
751 following lines were newly generated for this study: *Tg(10xUAS:myrGCaMP6s)*,
752 *Tg(olig1:myrGCaMP6s), Tg(10xUAS:myrGFP), Tg(10xUAS:myrmScarletI-p2A-Cas9, U6:ctrl-*
753 *sgRNA1;U6:ctrl-sgRNA2), Tg(10xUAS:myrmScarletI-p2A-Cas9, U6:nlgn3a*^{ex1}*-*
754 *sgRNA;U6:nlgn3a*^{ex4}*-sgRNA), Tg(10xUAS:myrmScarletI-p2A-Cas9, U6:nlgn3b*^{ex1}*-*

755 *sgRNA;U6:nlgn3b^{ex3}-sgRNA).* All experimental fish were crossed into the *nacre* background for
756 optimal optics without pigmentation. The Kalta4/UAS system allowed sparse labeling and single
757 cell analysis. The genotypes of fish used for each experiment are indicated in figure legends.
758 Animals in the fish facility were maintained at 28° C with a 14 h/10 h light/dark cycle. Larvae
759 and juveniles were nurtured with rotifer suspension and dry food (Gemma 75 and 150,
760 respectively). Adults were fed with a combination of brine shrimp and dry food (Gemma 300).
761 Male and female fish of 3 to 12 months-old were mated; larval fish of 2 dpf to 14 dpf were used
762 for experiments (sex is not determined at these stages in zebrafish). All zebrafish experiments
763 and procedures were performed in compliance with institutional ethical regulations for animal
764 testing and research at Oregon Health and Science University (OHSU). Experiments were
765 approved by the Institutional Animal Care and Use Committee of OHSU. Animal and cell
766 numbers are indicated in figure legends.
767
768 **METHOD DETAILS**
769 **Tissue sectioning and immunohistochemistry**
770 To prepare sagittal and transverse sections, zebrafish larvae at indicated stages were first
771 anesthetized with tricaine and then fixed in 4% PFA, 0.1% Triton at 4° C overnight. Heads and
772 tails were removed to enable better penetration of fixative. The fish were then washed in PBS,
773 0.1% Triton for 5 minutes and passed in 10%, 20%, and 30% sucrose in PBS, followed by OCT
774 embedding and cryosectioning of 20-25 µm slices. The sections were brought to room
775 temperature for 45 minutes and rehydrated in PBS, 0.2% Triton for 1 hour. 3% BSA, 5% NGS, 0.2%
776 Triton in PBS was used as blocking buffer. Primary antibodies: chicken anti-GFP (Invitrogen

777 A10262), 1:1000, mouse anti-Pan-MAGUK (NeuroMab K28/86) 1:500, mouse anti-Gephyrin
778 (Synaptic Systems 147011) 1:1000, rabbit anti-Synapsin 1/2 (Synaptic Systems 106002) 1:1000,
779 mouse anti PSD-95 6G6-1C9 (MAB1596) 1:1000, Rabbit anti-Glycine receptor (Synaptic Systems
780 146008) 1:1000. Secondary antibodies: A488 anti-chicken, A594 anti-rabbit, A647 anti-mouse
781 IgGI, A647 anti-mouse (Thermo Fisher). The stained samples were mounted in prolong Glass
782 (Invitrogen P36980) for at least a day before imaging.

783 **Plasmid construction**

784 In zebrafish, *gephyrin* is duplicated (*gephyrina* and *gephyrinb*), and there are multiple isoforms
785 for both genes. All isoforms are almost identical in protein sequence except for the inclusion or
786 exclusion of C3 and C4 cassettes. We amplified several isoforms from cDNA and decided to
787 follow up two: *gephyrinb* isoform X6 (XM_021468341) because it encodes a protein that is 96%
788 identical and 98% similar to the rat P1 isoform (NP_074056.2)[48] that has been used to track
789 synapses previously; and, *gephyrina* isoform X11 (XM_017351650.2) because it contains a C3
790 cassette previously reported to be present in glia cells[49].

791 Total RNA was extracted from 3 dpf zebrafish AB larvae (50 fish) using RNAeasy Plus Kit
792 (Qiagen 74134). cDNA was synthesized using SuperScript IV Reverse Transcriptase (Invitrogen).
793 Two sets of primers (Supplementary Table 1) were used to clone the full length *gephyrina* and
794 *gephyrinb* using high fidelity Q5 DNA polymerase, followed by A-addition and TA cloning into
795 pCRII-TOPO backbones. Using Gibson assembly (NEB E5510S), we added EGFP to the 5' end and
796 a linker GGGGSGGGGSGGGGS in between, and integrated it into pCS 2.1 backbones with an
797 AVRII digestion site. The 5' end was chosen based on previous imaging studies[48]. In transient
798 injections, GFP-Gephyrina and GFP-Gephyrinb exhibited similar expression profiles; therefore,

799 we used GFP-Gephyrinb for our studies and refer to the GFP-3xGGGGS-Gephyrinb as GFP-
800 Gephyrinb throughout the manuscript. Using Gateway BP reaction (Invitrogen 11786100), we
801 generated pME_ATG-GFP-Gephyrinb-TAA. Using AVRII and KPNI-HF, we cut GFP-Gephyrinb
802 (without an ATG) from the pCS 2.1 backbone and inserted it in frame into p3E_p2A to generate
803 p3E_p2A-GFP-Gephyrinb-TGA-polyA.

804 *PSD-95/dlg4b* transcript NM_214728.1 encodes a protein that is 76% identical and 83%
805 similar to rat *Dlg4* (NP_062567.1) and was thus chosen for use in our studies. We added GFP to
806 the 3'end because N-terminal palmitoylation of PSD-95 is necessary for its synaptic localization,
807 and receptor clustering[50,51]. It was cloned from cDNA with primers (Supplementary Table 1)
808 similar to *gephyrin* as described above. We refer to PSD-95-3xGGGGS-GFP as PSD-95-GFP. We
809 generated pME_ATG-PSD-95-GFP-TAA and p3E_p2A-PSD-95-GFP-TGA-polyA constructs.

810 pCAG_FingR.GFP-Gephyrin-CCR5TC (Addgene 46296) and pCAG_FingR.GFP-PSD-95-
811 CCR5TC (Addgene 46295) were used to amplify the coding region with additional 5' zinc finger
812 binding sequence to regulate their expression[20], followed by BP reaction to generate
813 pME_zincfinger_FingR.GFP-PSD-95-CCR5TC and pME_zincfinger_FingR.GFP-Gephyrin-CCR5TC
814 constructs.

815 pME_myrGFP and pME_myrTagRFP-T were generated using PCR and BP reaction, using
816 Fyn myristoylation and palmitoylation domain. pGP-CMV-GCaMP6s (Addgene 40753) was used
817 as a template and 3 primers were used in a Q5 PCR (15 cycles at 71° C and 20 cycles at 72° C) to
818 amplify GCaMP6s and add a Kozak sequence, myr (Fyn myristoylation and palmitoylation
819 domain), attB1, and attB2 sequences. This PCR product was used to generate
820 pME_myrGCaMP6s-TAA using BP reaction.

821 We obtained multiple plasmids from Tol2 kits: pDestTol2pA2, pDONR221, p5E_10xUAS,
822 p3E_polyA, p3E_p2A[52], p5E_sox10$_{7.2kb}$[47], pDestTol2pACryGFP (pDestTol2GE),
823 pDestTol2pACrymCherry (pDestTol2RE).
824 Using Gateway LR reactions (Invitrogen 11791020), we generated the following
825 constructs: PA2-10xUAS:myrEGFP-PolyA, GE-10xUAS:myrGCaMP6s-TAA-polyA, PA2-
826 olig1:myrGCaMP6s-TAA-polyA, GE-10xUAS:GFP-Gephyrinb-TAA-polyA, RE-10xUAS:GFP-
827 Gephyrina-TAA-polyA, GE-10xUAS:PSD-95-GFP-TAA-polyA, PA2-sox10:myrTagRFP-T-P2A-GFP-
828 Gephyrinb-polyA, PA2-sox10:myrTagRFP-T-P2A-PSD95-GFP-polyA, GE-
829 10xUAS:zincfinger_FingR.GFP-PSD-95-CCR5TC, GE-10xUAS:zincfinger_FingR.GFP-Gephyrin-
830 CCR5TC. We used Mnx1:Gal4[53] to drive myrGCaMP6s expression in motor neurons. We used
831 Huc:Kalta4 [47], UAS:TeNTlc-tdtomato[32] to drive TeNTlc expression in neurons. All constructs
832 generated in this study were fully sequenced (except *sox10* and *olig1* promoters, which are well
833 established tools).
834 **Cell specific CRISPR/Cas9 plasmid construction and CRISPR/Cas9-mediated gene disruption**
835 We used 5xUAS:hsp70promoter-Cas9-T2A-GFP, U6:sgRNA1;U6:sgRNA2[54] (Addgene 74009) as a
836 backbone and performed the following modifications: replacement of the 5xUAS:hsp70
837 promoter with the 10xUAS:E1b-bactin-Kozak promoter because we found the original promoter
838 expressed in many non-specific cell types when injected into *Tg(sox10:Kalta4)*; replacement of
839 T2A-GFP with myrmScarletI-p2A and added to the 5'end of Cas9; addition of polyA to the 3' end
840 of Cas9. Four sets of primers and 2 previously made plasmids (Tol2-10xUAS:E1b-mScarletI and
841 Tol2-10xUAS:cas9-P2A-TagRFPTcaax) were used to generate 4 segments. These segments were

842 integrated into the backbone by NEBuilder HiFi assembly (NEB E2621S). The new construct is
843 referred to as 10xUAS:myrmScarletI-p2A-Cas9, U6:sgRNA1;U6:sgRNA2.
844 CHOPCHOP and Crisprscan were used to identify 2 sgRNA sequences for each gene of
845 interest: *gephyrina* exon 2, GGTCATGAACGAGATCTTTGAGG; *gephyrinb* exon 7,
846 GGAGAGCCGGCAGGATGAACTGG; *myrf* exon 3, GACCCAACGGCGGTGCACCCGGG; *myrf* exon 4,
847 GCTGGAGTCCGGAGGAGACTCGG; *nlgn3a* exon 1, GGTGTATGATGCTTGTCCGGGGG; *nlgn3a* exon
848 4, GCCTTGTGTACTTAACCGGCTGG; *nlgn3b* exon 1, GATGCGGGTCGCTGTTGCCACGG; *nlgn3b*
849 exon 3, GGTAGTGTGCTGGCCAGCTACGG. The cutting efficiencies of these sgRNAs were verified
850 (>95%) via enzyme digestion of the targeted locus PCR product (CRISPRtest primers, Fig. S3E).
851 F0 larvae with *gephyrina* and *gephyrinb* sgRNA injected together with 1 ng Cas9 protein were
852 used to examine the specificity of the Gephyrin antibody. BsaI and BsmBI were used to insert
853 the sgRNA into 10xUAS:myrmScarletI-p2A-Cas9, U6:sgRNA1;U6:sgRNA2. The plasmids were
854 injected with Tol2 transposase mRNA to generate transgenic fish. *Tg(10xUAS:myrmScarletI-*
855 *p2A-Cas9, U6:myrf^{exon3};U6:myrf^{exon4}), Tg(10xUAS:myrmScarletI-p2A-Cas9,*
856 *U6:nlgn3a^{exon1};U6:nlgn3a^{exon4})*, and *Tg(10xUAS:myrmScarletI-p2A-Cas9,*
857 *U6:nlgn3b^{exon1};U6:nlgn3b^{ex34})* larvae with sparsely labeled oligodendrocyte were examined for
858 morphology and sheath characteristics. *Tg(10xUAS:myrmScarletI-p2A-Cas9,*
859 *U6:sgRNA1;U6:sgRNA2)* larvae were used as controls.
860 **Sparse labeling and generation of transgenic lines**
861 Fertilized zebrafish eggs at the 1-cell stage zebrafish zygotes were microinjected with 1 nL of
862 an injection solution containing 20 ng/µL plasmid DNA, 25 ng/µL Tol2 transposase mRNA, 0.02%
863 phenol red and 0.2M KCl. Injected F0 animals were either used for single-cell analysis or raised

864 to adulthood to generate transgenic lines. To generate stable lines, F1 progenies were screened
865 for germline transmission of the fluorescent reporters. F1 animals were further outcrossed and
866 maintained in the *nacre* background to establish stable transgenic lines with single copy
867 insertion.

868 **Mounting larvae for *in vivo* imaging**

869 For most live imaging experiments, larvae were anesthetized with 0.16 mg/mL (600 µM)
870 tricaine in embryo medium. The fish were mounted in 0.8% low melting agarose (Sigma A9414)
871 on a coverslip for morphology and sheath examination or in 1.5% low melting agarose in a dish
872 for time lapse imaging (hours). For Gephyrin hotspot and myrGCaMP6s imaging, larvae were
873 immobilized with 0.5 mg/ml non-depolarizing acetylcholine receptor antagonist mivacurium
874 chloride (Abcam) and mounted in 1.5% low melting agarose in a dish.

875 **Confocal microscopy**

876 All imaging was performed on an upright Zeiss LSM 980 confocal with Airyscan 2 in 4Y fast
877 mode. For fixed tissues, a 63x/1.4 NA oil objective was used, and for live imaging, a 20x/1.0 NA
878 water objective was used. All images were taken in Zeiss software. We used the following lasers:
879 488 nm for EGFP, myrGCaMP6s, and Alexa488; 561 nm for TagRFP, mScarletI, tdtomato, and
880 Alexa594; 639 nm for Alexa647. Fixed tissue was imaged with 0.15 µm z spacing with 1.6x to
881 2.5x zoom. For *in vivo* analyses, PSD-95-GFP and GFP-Gephyrin were imaged with 2 µm z-
882 spacing at an interval of 5 min (for 30 min to 1 hour) or 20 min (for longer than 1 hour) at a
883 zoom between 3.7x-10x depending on OPC cell size. myrGCaMP6s was imaged with 2 µm z-
884 spacing at 0.5 Hz (4 planes scanned) for 10 min or 20 min (drug injection experiments) as
885 previously described[17,18]. Images acquired at 0.5 Hz were analyzed along with images acquired

886 at 10 Hz with a single plane. No major differences were found on the Ca^{2+} spike characteristics,
887 but 0.5 Hz acquisition allowed inclusion of more stacks and increased the number of events
888 detected. Therefore, 0.5 Hz was used throughout the study. For tracking OPCs that differentiate
889 into myelinating oligodendrocyte, Ca^{2+} imaging was done repeatedly for 5 min at the beginning
890 of each hour.

891 **Drug delivery through ventricle injection**

892 For myrGCaMP6s experiments involving drug delivery, we injected drugs via ventricle injection
893 as described previously[18]. In TTX treatment, following 10 min GCaMP6s imaging, a 1 nL mixture
894 containing 0.2M KCL, 0.5% Dextran Texas Red 3000 MW (Thermo), and molecular biology grade
895 H_2O (control) or TTX (0.5 mM, kind gifts from Henrique von Gersdorff's lab) were pressure
896 injected into the hindbrain ventricle using an ASI MPPI-3. Between 15 and 35 min after injection,
897 Dextran was imaged, followed by another 10 min of GCaMP6s imaging. Dextran surrounding
898 the imaged OPCs was used to verify the drug delivery. TTX caused fish paralysis, further
899 verifying efficient delivery of active drugs. After imaging, fish were removed from mounting
900 media. Larvae injected with control solution recovered full swimming activity within 3 minutes,
901 and TTX-injected paralyzed larvae maintained normal heartbeats for at least 3 hours. In TeNT
902 treatment, an 8 nL mixture containing 0.2M KCL, 0.5% Dextran Antonia Red 150,000 MW
903 (Sigma), and TeNT (listlabs 190A, 0.5 µM) were pressure injected into the hindbrain ventricle.
904 Between 50 and 70 min after injection, Dextran was imaged, followed by another 10 min of
905 GCaMP6s imaging. TeNT-injected larvae showed reduced swimming activity.

906

907 **QUANTIFICATION AND STATISTICAL ANLYSIS**

908 **OPC labeling during development**

909 We used *sox10* and *olig1* to label OPCs. *sox10* drives expression in both OPCs and myelinating
910 oligodendrocytes while *olig1* labels only OPCs. OPCs and myelinating oligodendrocytes could be
911 distinguished by cell morphology: OPCs only possessed processes and myelinating
912 oligodendrocytes possessed sheaths. Animal ages and corresponding OPC activity: 2 dpf (when
913 OPCs are born, and migrate), 3 dpf (when many OPCs initiate differentiation), 5-14 dpf (when
914 many OPCs complete differentiation.)

915 **Alignment rate and colocalization ratio**

916 Images of fixed tissue were analyzed in Imaris. "Surface" function was used to create a cell
917 surface (Smooth and Surface Grain Size = 0.0850 µm; Diameter of Largest Sphere = 5 µm;
918 Threshold between 900-1200; Number of Voxels above 100). "Spot" function was used to
919 generate $Spot_{postsynaptic\ puncta}$ (Estimated XY Diameter = 0.35 µm; Estimated Z Diameter = 0.5 µm;
920 Background subtraction; quality above 2500 to 2800). Then the cell surface was used as a mask
921 to generate $Spot_{postsynaptic\ puncta\ in\ OPCs}$, which was further verified by crosschecking its overlap
922 with $Spot_{postsynaptic\ puncta}$. $Spot_{postsynaptic\ puncta\ in\ OPCs}$ was analyzed for puncta number or density. To
923 examine the alignment of MAGUK (Gephyrin) and Synapsin, we used "Spot" function to
924 generate $Spot_{Synapsin\ puncta}$. By determining the proximity $Spot_{postsynaptic\ puncta\ in\ OPCs}$ to $Spot_{Synapsin}$
925 $_{puncta}$ using MATLAB-enabled "Colocalize Spots" function (<0.1 µm), we could identify
926 postsynaptic puncta in OPCs that aligned with Synapsin and calculate the alignment rate. To
927 calculate the colocalization ratio of MAGUK (Gephyrin)-Synapsin, we used the Imaris "Coloc"
928 function to generate a new M&S coloc channel based on the overlapping pixels between
929 MAGUK (Gephyrin) and Synapsin channel above thresholds. "Surface" function was used to

930 generate M&S coloc surface of the whole section, MAGUK (Gephyrin) (M) surface of the whole
931 section, and OPC surface. OPC surface was used as a mask to generate masked M&S coloc
932 channel and MAGUK (Gephyrin) channel. These masked channels were then used to generate
933 M&S coloc surface In OPCs and M surface in OPCs." The colocalization ratio in OPCs and
934 neurons was calculated as follows:

935 $$\boldsymbol{Colocalization\ ratio_{OPCs}} = \frac{\boldsymbol{Volume_{M\&S\ coloc\ surface\ in\ OPCs}}}{\boldsymbol{Volume_{M\ surface\ in\ OPCs}}};$$

936 $$\boldsymbol{Colocalization\ ratio_{neurons}} =$$

937 $$\frac{\boldsymbol{Volume_{M\&S\ coloc\ surface\ of\ the\ whole\ section} - Volume_{M\&S\ coloc\ surface\ in\ OPCs}}}{\boldsymbol{Volume_{M\ surface\ of\ the\ whole\ section} - Volume_{M\ Surface\ in\ OPCs}}}.$$

938 **Postsynaptic puncta identification and analysis**

939 Live Images of PSD-95-GFP and GFP-Gephyrin were processed in ImageJ, and synaptic puncta
940 were identified and tracked with Trackmate[55]. The images were first maximally projected and
941 stabilized using "Image Stabilizer." In Trackmate, parameters were set as follows: LOG mode,
942 diameter 0.75 µm, Quality>100, contrast>0.19 and signal noise >0.35, LAP linking with 0.5 µm
943 distance and 2 max gap frames allowed were applied. The identified puncta at each frame were
944 then manually examined to remove poor quality tracks. Neighboring puncta may sometimes be
945 incorrectly linked between timelapses; therefore, manual examinations were done to fix these
946 link errors. The data output was analyzed in MATLAB with custom scripts to calculate puncta
947 number per cell at each timepoint, puncta duration and diameter. To generate Fig.s of mean
948 and standard deviation as shade, we used a modified script
949 (https://www.mathworks.com/matlabcentral/fileexchange/29534-stdshade). To analyze the
950 puncta number during OPC differentiation, time points when OPC shows first sheath

951 (differentiation) and when myelinating oligodendrocyte's last process disappeared and all
952 process transformed into sheaths (maturation) were noted for each cell. In MATLAB, this
953 information is used to divide the puncta number into before and after differentiation or
954 maturation for each cell. The traces were generated after the data was realigned to set the
955 timepoint of differentiation or maturation as time 0.

956 **Hotspot analysis**

957 Heatmaps of puncta over time were generated using the output data with Heatscatter
958 (https://www.mathworks.com/matlabcentral/fileexchange/47165-heatscatter-plot-for-
959 variables-x-and-y). With a sampling volume of 1 x 1 x 4 µm, regions with frequency higher than
960 3 standard deviations were identified as hotspots using custom MATLAB scripts, which also
961 measured the distance between the center of hotspots and future sheaths. In time-lapse
962 imaging that encompassed both OPC and oligodendrocyte stages, we used the first nascent
963 sheath appearance (time 0) to separate OPC stage and oligodendrocyte stage. In some cases,
964 the first nascent sheath appeared between our observation timepoints or disappeared for half
965 an hour; therefore, we decided to confine the OPC stage up to one hour before time 0. The
966 distances between hotspots and myelin sheaths were measured using custom MATLAB scripts.
967 To choose 5-30 representative points outside hotspots in an OPC, we first used Trackmate to
968 identify 80-400 points along OPC processes (not soma) using the RFP channel. We removed the
969 points that are within 5 µm from the hotspot centers in the OPC and clustered the rest of points
970 into 5-30 groups (nonhotspots) using Lloyd's algorithm in MATLAB. Then we measured the
971 distances from each nonhotspot center to its closest myelin sheaths within the same OPC. To
972 examine how hotspots or nonhotspots predicted myelin sheaths, we analyzed the frequency

973 distribution of hotspot-sheath and nonhotspot-sheath distances, and calculated the percentage
974 of distances that were less than 1 µm.

975 **Ca^{2+} events analysis**

976 myrGCaMP6s images of z-stacks were maximum projected and stabilized using "Image
977 Stabilizer." The images were assigned with random names using "blindr"
978 (https://github.com/U8NWXD/blindr) before analysis and reassigned with the original names
979 after analysis. The regions of Ca^{2+} events (ROI) were identified by "GECIquant"[56] first and then
980 manually examined frame by frame. The intensity and area of each ROI were exported and
981 processed in MATLAB through custom scripts. Briefly, $\Delta F/F_{average}$ ($\Delta F=F- F_{average}$) was calculated
982 to generate traces and to identify intensity peaks using "findpeaks" in MATLAB with filtering
983 parameters (3 standard deviations above average, prominence larger than 40% of the baseline,
984 and peak area larger than 2.5). Rare elevated Ca^{2+} signal for extended periods of time (longer
985 than 50 seconds) were excluded. Peaks were manually verified against the image. Several Ca^{2+}
986 characteristics were measured: peak amplitude, peak duration, Ca^{2+} MD number, Ca^{2+} MD area,
987 and frequency of Ca^{2+} activity. A region with multiple OPCs was analyzed for TeNTlc and TeNT
988 experiment, while single OPCs were analyzed for the rest of experiments. To examine the
989 proximity of synaptophysin-TagRFP to Ca^{2+} MD, Ca^{2+} MDs were identified as above, and their
990 locations were first compared to synaptophysin-TagRFP manually plane by plane and then
991 verified by Imaris. In Imaris, using "Spot" and "Surface" functions, we generated synaptophysin-
992 TagRFP puncta and OPC surface, with which we identified the puncta that were close to OPC
993 surfaces using a MATLAB-enabled "Spot-to-Surface" function (0.1 µm threshold). These puncta
994 were manually checked against Ca^{2+} MDs identified through morphological landmarks in Imaris.

995 The distance between Ca^{2+} and future sheaths were measured in MATLAB. In TeNTlc
996 experiments, the number of axons expressing TeNTlc-tdtomato was counted in each image. If
997 the number was less than 4, the corresponding image was grouped as "neighboring few TeNTlc
998 axons"; otherwise, the image was grouped as "neighboring many TeNTlc axons". The distances
999 between Ca^{2+} MDs and future myelin sheaths were measured using custom MATLAB scripts. To
1000 choose 5-30 representative points outside MDs in an OPC, we first used Trackmate to identify
1001 80-400 points along OPC processes (not soma) using the RFP channel. We removed the points
1002 that are within 5 µm from the MD centers in the OPC and clustered the rest of points into 5-30
1003 groups (nonMDs) using Lloyd's algorithm in MATLAB. Then we measured the distances from
1004 each nonMD center to its closest myelin sheaths within the same OPC. To examine how MDs or
1005 nonMDs predicted myelin sheaths, we analyzed the frequency distribution of MD-sheath and
1006 nonMD-sheath distances, and calculated the percentage of distances that were less than 1 µm.
1007

1008 **Oligodendrocyte and myelin sheath analysis**

1009 To analyze myelin sheath length and number, we used ImageJ ROI manager to trace all sheaths
1010 of sparsely labeled oligodendrocytes between segments 1 and 15 in spinal cord. The number of
1011 oligodendrocytes analyzed per fish was limited to 3 to ensure even weight among individual fish.
1012 Sheath traces and the corresponding images were blinded using "File Name Encrypter" in
1013 ImageJ. The sheath length and number were then analyzed in MATLAB with custom scripts and
1014 matched with the original genotype following analysis. To calculate the oligodendrocyte %, in
1015 each imaging experiment, the number of oligodendrocytes from one genotype was counted
1016 and divided to the total number of cells (both oligodendrocytes and OPCs).

1017 **Statistics**

1018 Most data are shown as mean ± SEM., with individual data points shown as circles. We
1019 conducted Shapiro-Wilk's test and Levene's test to verify data normality and homoscedasticity,
1020 respectively, before performing two-sided *t*-test for unpaired groups, paired *t*-test for paired
1021 groups, and one-way ANOVA and Tukey's test for more than 3 groups. If the data did not pass
1022 normality tests, we used Kruskal-Wallis test for more than 3 groups and Mann-Whitney test for
1023 2 groups. These analyses were performed either in GraphPad Prism or MATLAB. The
1024 significance and statistical analyses employed were indicated in Fig. legends. Animal and cell
1025 number used for each experiment, t-values and df for *t*-tests, and *F* values and df for ANOVA
1026 were indicated in figure legends. Data collection was not performed blindly due to the
1027 experimental conditions, but analyses were performed blindly as indicated. Sample size was
1028 chosen based on standard deviation and effect (http://www.biomath.info/power/ttest.htm).
1029 Sex is not yet determined in zebrafish at the ages employed in our study and so cannot be
1030 considered as a biological variable.

1031

1032 **Reporting summary**

1033 Further information on research design is available in the Nature Research Reporting Summary
1034 linked to this manuscript.

1035

1036 **Data availability**

1037 All research materials are available upon request. Source data are provided with this paper.

1038

1039 **Code availability**

1040 All custom scripts are available upon request.

1041

1042 ## REFERENCES

1043 1. Franklin, R. J. M. & Ffrench-Constant, C. Remyelination in the CNS: From biology to

1044 therapy. *Nature Reviews Neuroscience* vol. 9 839–855 (2008).

1045 2. Xiao, Y., Petrucco, L., Hoodless, L. J., Portugues, R. & Czopka, T. Oligodendrocyte

1046 precursor cells sculpt the visual system by regulating axonal remodeling. *Nat. Neurosci.*

1047 **25**, 280–284 (2022).

1048 3. Venkatesh, H. S. *et al.* Targeting neuronal activity-regulated neuroligin-3 dependency in

1049 high-grade glioma. *Nature* **549**, 533–537 (2017).

1050 4. Bergles, D. E. & Richardson, W. D. Oligodendrocyte development and plasticity. *Cold*

1051 *Spring Harb. Perspect. Biol.* **8**, a020453 (2016).

1052 5. Lundgaard, I. *et al.* Neuregulin and BDNF Induce a Switch to NMDA Receptor-Dependent

1053 Myelination by Oligodendrocytes. *PLoS Biol.* **11**, (2013).

1054 6. de Biase, L. M. *et al.* NMDA receptor signaling in oligodendrocyte progenitors is not

1055 required for oligodendrogenesis and myelination. *J. Neurosci.* **31**, 12650–12662 (2011).

1056 7. Zonouzi, M. *et al.* GABAergic regulation of cerebellar NG2 cell development is altered in

1057 perinatal white matter injury. *Nat. Neurosci.* **18**, 674–682 (2015).

1058 8. Balia, M., Benamer, N. & Angulo, M. C. A specific GABAergic synapse onto

1059 oligodendrocyte precursors does not regulate cortical oligodendrogenesis. *Glia* **65**, 1821–

1060 1832 (2017).

1061 9. Mitew, S. *et al.* Pharmacogenetic stimulation of neuronal activity increases myelination
1062 in an axon-specific manner. *Nat. Commun.* **9**, 306 (2018).
1063 10. Hines, J. H., Ravanelli, A. M., Schwindt, R., Scott, E. K. & Appel, B. Neuronal activity biases
1064 axon selection for myelination in vivo. *Nat. Neurosci.* **18**, 683–689 (2015).
1065 11. Gibson, E. M. *et al.* Neuronal activity promotes oligodendrogenesis and adaptive
1066 myelination in the mammalian brain. *Science (80-.).* **344**, (2014).
1067 12. Mensch, S. *et al.* Synaptic vesicle release regulates myelin sheath number of individual
1068 oligodendrocytes in vivo. *Nat. Neurosci.* **18**, 628–630 (2015).
1069 13. Nagy, B., Hovhannisyan, A., Barzan, R., Chen, T. J. & Kukley, M. Different patterns of
1070 neuronal activity trigger distinct responses of oligodendrocyte precursor cells in the
1071 corpus callosum. *PLoS Biol.* **15**, (2017).
1072 14. Barron, T. & Kim, J. H. Neuronal input triggers Ca2+ influx through AMPA receptors and
1073 voltage-gated Ca2+ channels in oligodendrocytes. *Glia* **67**, 1922–1932 (2019).
1074 15. Sun, W., Matthews, E. A., Nicolas, V., Schoch, S. & Dietrich, D. Ng2 glial cells integrate
1075 synaptic input in global and dendritic calcium signals. *Elife* **5**, (2016).
1076 16. Hamilton, N., Vayro, S., Wigley, R. & Butt, A. M. Axons and astrocytes release ATP and
1077 glutamate to evoke calcium signals in NG2-glia. *Glia* **58**, 66–79 (2010).
1078 17. Marisca, R. *et al.* Functionally distinct subgroups of oligodendrocyte precursor cells
1079 integrate neural activity and execute myelin formation. *Nat. Neurosci.* **23**, 363–374
1080 (2020).
1081 18. Krasnow, A. M., Ford, M. C., Valdivia, L. E., Wilson, S. W. & Attwell, D. Regulation of
1082 developing myelin sheath elongation by oligodendrocyte calcium transients in vivo. *Nat.*

1083 *Neurosci.* **21**, 24–30 (2018).

1084 19. Zhang, Y. *et al.* An RNA-sequencing transcriptome and splicing database of glia, neurons,
1085 and vascular cells of the cerebral cortex. *J. Neurosci.* **34**, 11929–11947 (2014).

1086 20. Gross, G. G. *et al.* Recombinant Probes for Visualizing Endogenous Synaptic Proteins in
1087 Living Neurons. *Neuron* **78**, 971–985 (2013).

1088 21. Hughes, A. N. & Appel, B. Oligodendrocytes express synaptic proteins that modulate
1089 myelin sheath formation. *Nat. Commun.* **10**, (2019).

1090 22. Marques, S. *et al.* Oligodendrocyte heterogeneity in the mouse juvenile and adult central
1091 nervous system. *Science (80-.).* **352**, 1326–1329 (2016).

1092 23. Spitzer, S. O. *et al.* Oligodendrocyte Progenitor Cells Become Regionally Diverse and
1093 Heterogeneous with Age. *Neuron* **101**, 459-471.e5 (2019).

1094 24. Yoshii, A. & Constantine-Paton, M. BDNF induces transport of PSD-95 to dendrites
1095 through PI3K-AKT signaling after NMDA receptor activation. *Nat. Neurosci.* **10**, 702–711
1096 (2007).

1097 25. Meier, J. & Grantyn, R. A Gephyrin-Related Mechanism Restraining Glycine Receptor
1098 Anchoring at GABAergic Synapses. *J. Neurosci.* **24**, 1398–1405 (2004).

1099 26. Nikonenko, I. *et al.* PSD-95 promotes synaptogenesis and multiinnervated spine
1100 formation through nitric oxide signaling. *J. Cell Biol.* **183**, 1115–1127 (2008).

1101 27. Kukley, M., Nishiyama, A. & Dietrich, D. The fate of synaptic input to NG2 glial cells:
1102 Neurons specifically downregulate transmitter release onto differentiating
1103 oligodendroglial cells. *J. Neurosci.* **30**, 8320–8331 (2010).

1104 28. De Biase, L. M., Nishiyama, A. & Bergles, D. E. Excitability and synaptic communication

1105 within the oligodendrocyte lineage. *J. Neurosci.* **30**, 3600–3611 (2010).

1106 29. Czopka, T., ffrench-Constant, C. & Lyons, D. A. Individual oligodendrocytes have only a
1107 few hours in which to generate new myelin sheaths invivo. *Dev. Cell* **25**, 599–609 (2013).

1108 30. Hildebrand, D. G. C. *et al.* Whole-brain serial-section electron microscopy in larval
1109 zebrafish. *Nature* **545**, 345–349 (2017).

1110 31. Baraban, M., Koudelka, S. & Lyons, D. A. Ca 2+ activity signatures of myelin sheath
1111 formation and growth in vivo. *Nat. Neurosci.* **21**, 19–25 (2018).

1112 32. Koudelka, S. *et al.* Individual Neuronal Subtypes Exhibit Diversity in CNS Myelination
1113 Mediated by Synaptic Vesicle Release. *Curr. Biol.* **26**, 1447–1455 (2016).

1114 33. Krueger-Burg, D., Papadopoulos, T. & Brose, N. Organizers of inhibitory synapses come of
1115 age. *Curr. Opin. Neurobiol.* **45**, 66–77 (2017).

1116 34. Almeida, A. R. & Macklin, W. B. Early myelination involves the dynamic and repetitive
1117 ensheathment of axons which resolves through a low and consistent stabilization rate.
1118 *bioRxiv* 2022.07.17.500324 (2022) doi:10.1101/2022.07.17.500324.

1119 35. Osso, L. A., Rankin, K. A. & Chan, J. R. Experience-dependent myelination following stress
1120 is mediated by the neuropeptide dynorphin. *Neuron* **109**, 3619-3632.e5 (2021).

1121 36. Almeida, R. G. *et al.* Myelination induces axonal hotspots of synaptic vesicle fusion that
1122 promote sheath growth. *Curr. Biol.* **31**, 3743-3754.e5 (2021).

1123 37. Gerrow, K. *et al.* A preformed complex of postsynaptic proteins is involved in excitatory
1124 synapse development. *Neuron* **49**, 547–562 (2006).

1125 38. Panzer, J. A. *et al.* Neuromuscular synaptogenesis in wild-type and mutant zebrafish. *Dev.*
1126 *Biol.* **285**, 340–357 (2005).

1127 39. Wierenga, C. J., Becker, N. & Bonhoeffer, T. GABAergic synapses are formed without the
1128 involvement of dendritic protrusions. *Nat. Neurosci.* **11**, 1044–1052 (2008).
1129 40. Villa, K. L. *et al.* Inhibitory Synapses Are Repeatedly Assembled and Removed at
1130 Persistent Sites In Vivo. *Neuron* **89**, 756–769 (2016).
1131 41. Wake, H., Lee, P. R. & Fields, R. D. Control of local protein synthesis and initial events in
1132 myelination by action potentials. *Science (80-.).* **333**, 1647–1651 (2011).
1133 42. Proctor, D. T. *et al.* Axo-glial communication through neurexin-neuroligin signaling
1134 regulates myelination and oligodendrocyte differentiation. *Glia* **63**, 2023–2039 (2015).
1135 43. Stogsdill, J. A. *et al.* Astrocytic neuroligins control astrocyte morphogenesis and
1136 synaptogenesis. *Nature* **551**, 192–197 (2017).
1137 44. Waggener, C. T., Dupree, J. L., Elgersma, Y. & Fuss, B. CaMKIIβ regulates oligodendrocyte
1138 maturation and CNS myelination. *J. Neurosci.* **33**, 10453–10458 (2013).
1139 45. Mitra, S. K., Hanson, D. A. & Schlaepfer, D. D. Focal adhesion kinase: In command and
1140 control of cell motility. *Nature Reviews Molecular Cell Biology* vol. 6 56–68 (2005).
1141 46. Venkatesh, H. S. *et al.* Neuronal activity promotes glioma growth through neuroligin-3
1142 secretion. *Cell* **161**, 803–816 (2015).
1143 47. Almeida, R. G. & Lyons, D. A. Intersectional gene expression in zebrafish using the split
1144 KalTA4 system. *Zebrafish* **12**, 377–386 (2015).
1145 48. Fuhrmann, J. C. *et al.* Gephyrin interacts with dynein light chains 1 and 2, components of
1146 motor protein complexes. *J. Neurosci.* **22**, 5393–5402 (2002).
1147 49. Smolinsky, B., Eichler, S. A., Buchmeier, S., Meier, J. C. & Schwarz, G. Splice-specific
1148 functions of gephyrin in molybdenum cofactor biosynthesis. *J. Biol. Chem.* **283**, 17370–

1149 17379 (2008).

1150 50. Craven, S. E., El-Husseini, A. E. & Bredt, D. S. Synaptic targeting of the postsynaptic

1151 density protein PSD-95 mediated by lipid and protein motifs. *Neuron* **22**, 497–509 (1999).

1152 51. Topinka, J. R. & Bredt, D. S. N-terminal palmitoylation of PSD-95 regulates association

1153 with cell membranes and interaction with K+ channel K(v)1.4. *Neuron* **20**, 125–134 (1998).

1154 52. Kwan, K. M. *et al.* The Tol2kit: A multisite gateway-based construction Kit for Tol2

1155 transposon transgenesis constructs. *Dev. Dyn.* **236**, 3088–3099 (2007).

1156 53. Wyart, C. *et al.* Optogenetic dissection of a behavioural module in the vertebrate spinal

1157 cord. *Nature* **461**, 407–410 (2009).

1158 54. Di Donato, V. *et al.* 2C-Cas9: A versatile tool for clonal analysis of gene function. *Genome*

1159 *Res.* **26**, 681–692 (2016).

1160 55. Tinevez, J. Y. *et al.* TrackMate: An open and extensible platform for single-particle

1161 tracking. *Methods* **115**, 80–90 (2017).

1162 56. Srinivasan, R. *et al.* Ca2+ signaling in astrocytes from Ip3r2 -/- mice in brain slices and

1163 during startle responses in vivo. *Nat. Neurosci.* **18**, 708–717 (2015).

1164

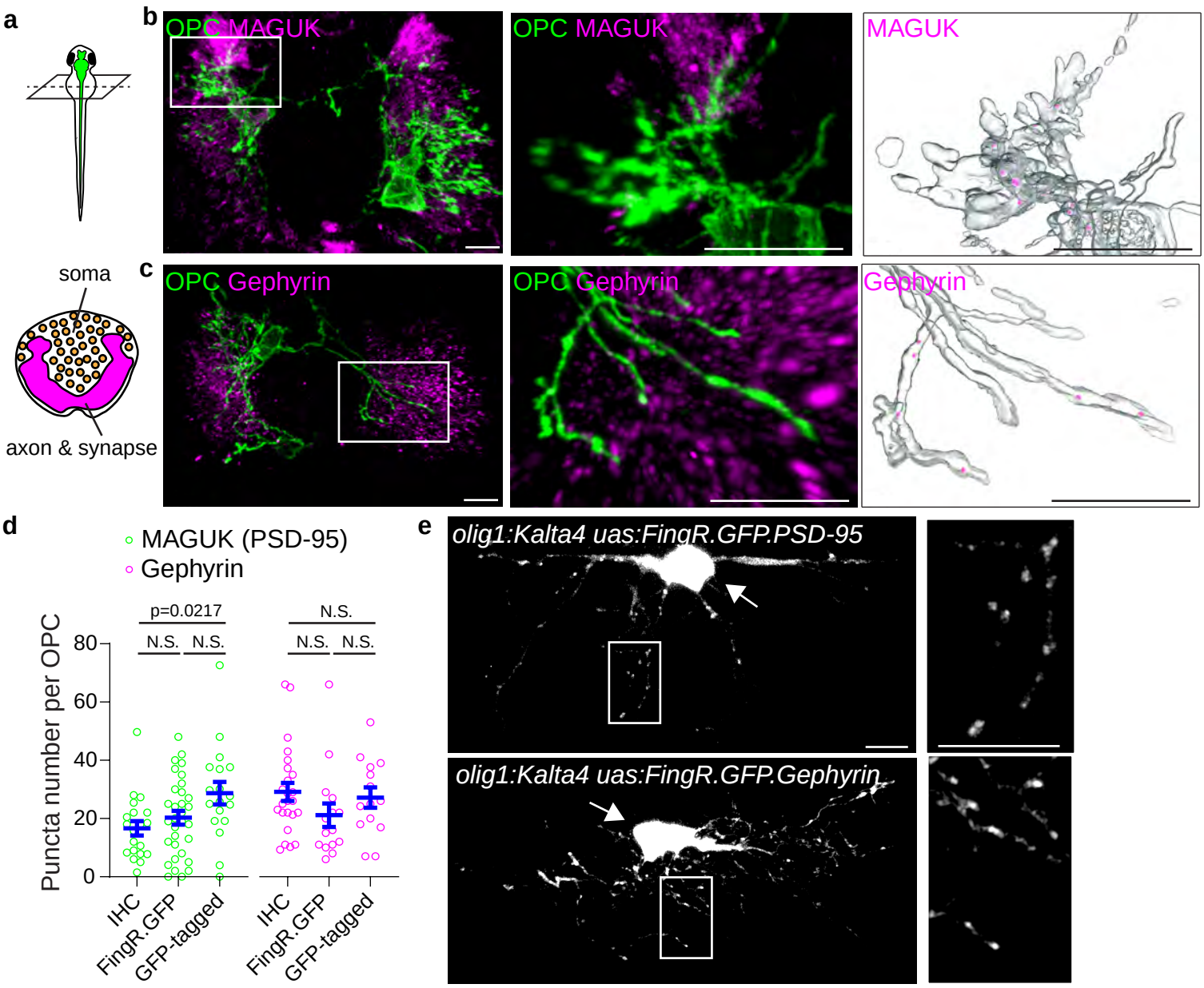
a
b
OPC MAGUK
OPC MAGUK
MAGUK
soma
axon & synapse
c
OPC Gephyrin
OPC Gephyrin
Gephyrin
d
MAGUK (PSD-95)
Gephyrin
p=0.0217
N.S.
N.S.
N.S.
N.S.
N.S.
Puncta number per OPC
80
60
40
20
0
IHC
FingR.GFP
GFP-tagged
IHC
FingR.GFP
GFP-tagged
e
olig1:Kalta4 uas:FingR.GFP.PSD-95
olig1:Kalta4 uas:FingR.GFP.Gephyrin

Figure 1

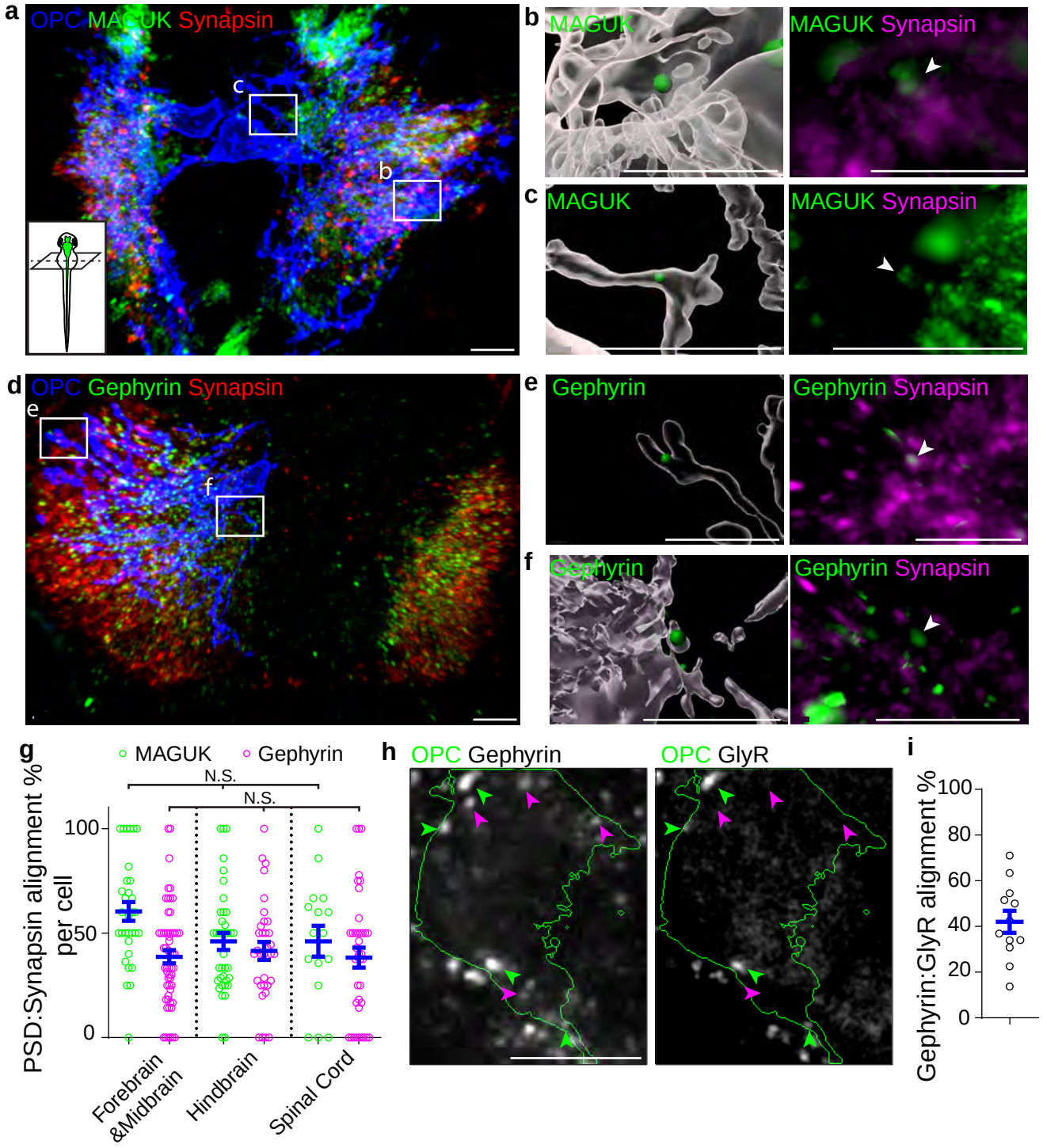
a
OPC MAGUK Synapsin
c
b
b
MAGUK
MAGUK Synapsin
c
MAGUK
MAGUK Synapsin
d
OPC Gephyrin Synapsin
e
f
e
Gephyrin
Gephyrin Synapsin
f
Gephyrin
Gephyrin Synapsin
g
MAGUK
Gephyrin
N.S.
N.S.
PSD:Synapsin alignment % per cell
100
50
0
Forebrain &Midbrain
Hindbrain
Spinal Cord
h
OPC Gephyrin
OPC GlyR
i
Gephyrin:GlyR alignment %
100
80
60
40
20
0

Figure 2

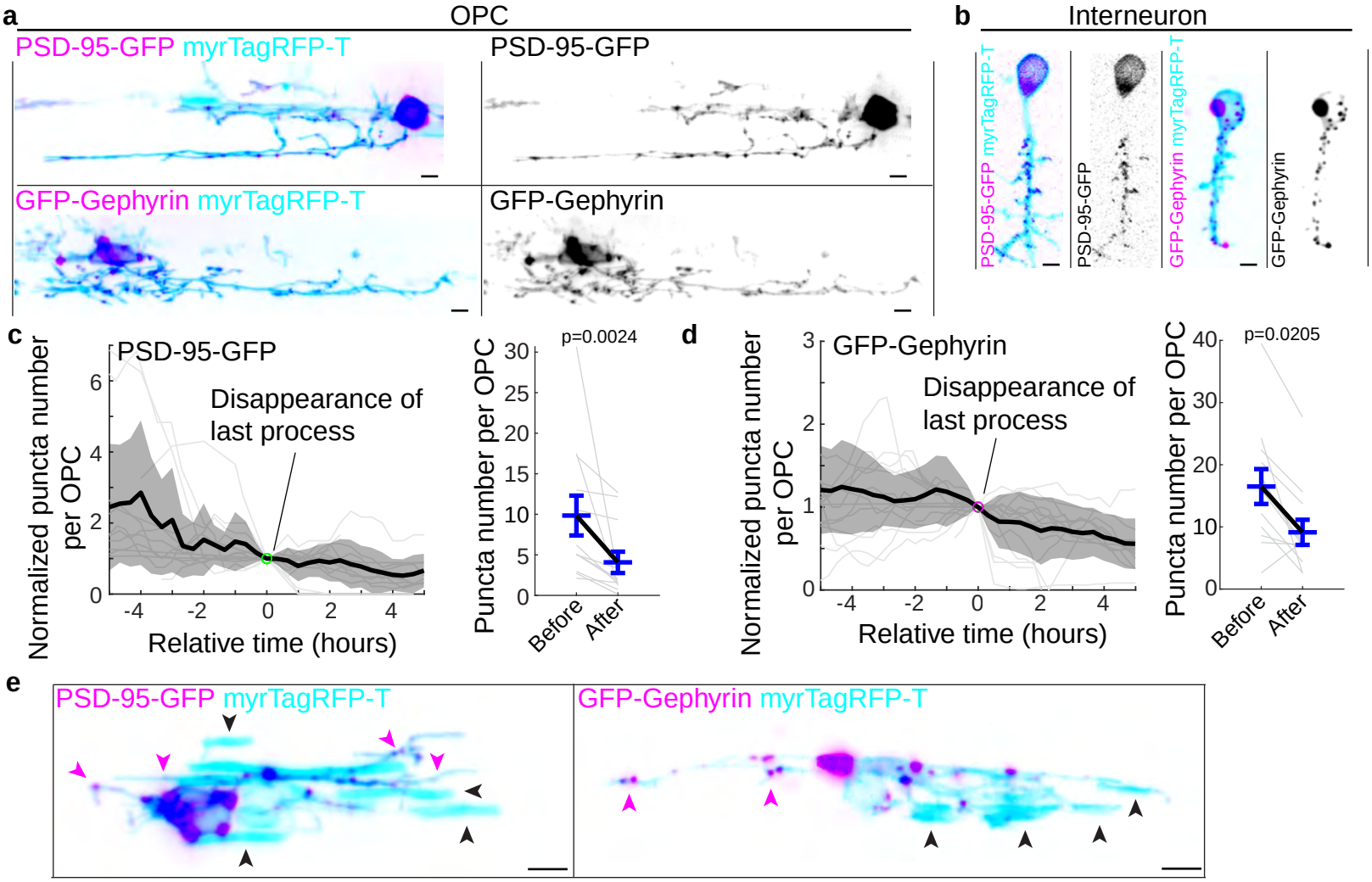
a
OPC
PSD-95-GFP myrTagRFP-T
PSD-95-GFP
GFP-Gephyrin myrTagRFP-T
GFP-Gephyrin
b
Interneuron
PSD-95-GFP myrTagRFP-T
PSD-95-GFP
GFP-Gephyrin myrTagRFP-T
GFP-Gephyrin
c
PSD-95-GFP
Disappearance of last process
Normalized puncta number per OPC
Relative time (hours)
Puncta number per OPC
p=0.0024
Before
After
d
GFP-Gephyrin
Disappearance of last process
Normalized puncta number per OPC
Relative time (hours)
Puncta number per OPC
p=0.0205
Before
After
e
PSD-95-GFP myrTagRFP-T
GFP-Gephyrin myrTagRFP-T

Figure 3

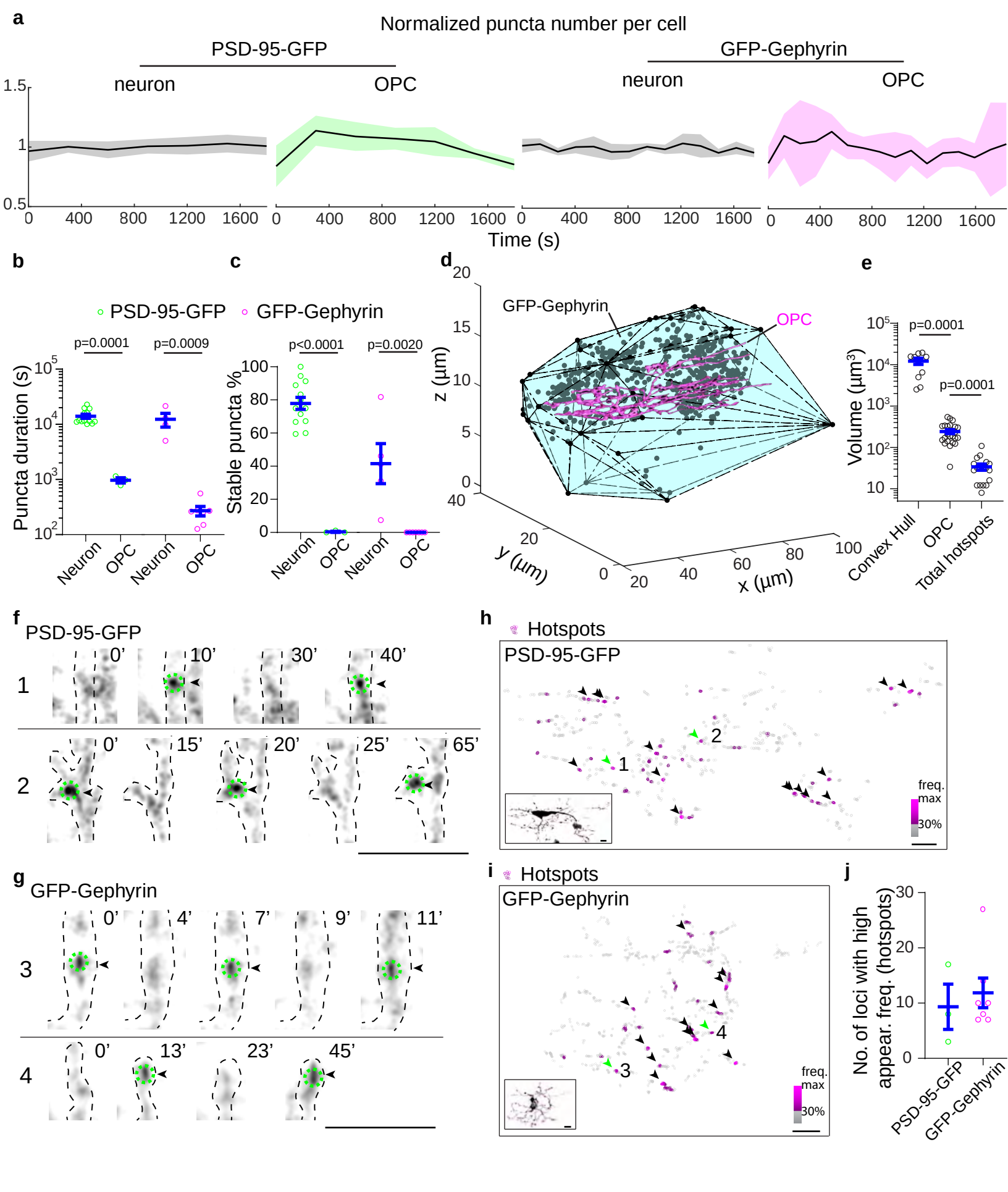
a
Normalized puncta number per cell
PSD-95-GFP
GFP-Gephyrin
neuron
OPC
neuron
OPC
1.5
1
0.5
0
400
800
1200
1600
Time (s)
b
PSD-95-GFP
GFP-Gephyrin
p=0.0001
p=0.0009
Puncta duration (s)
Neuron
OPC
Neuron
OPC
c
p<0.0001
p=0.0020
Stable puncta %
Neuron
OPC
Neuron
OPC
d
GFP-Gephyrin
OPC
z (µm)
y (µm)
x (µm)
e
p=0.0001
p=0.0001
Volume (µm³)
Convex Hull
OPC
Total hotspots
f
PSD-95-GFP
0'
10'
30'
40'
1
0'
15'
20'
25'
65'
2
g
GFP-Gephyrin
0'
4'
7'
9'
11'
3
0'
13'
23'
45'
4
h
Hotspots
PSD-95-GFP
1
2
freq.
max
30%
i
Hotspots
GFP-Gephyrin
3
4
freq.
max
30%
j
No. of loci with high appear. freq. (hotspots)
PSD-95-GFP
GFP-Gephyrin

Figure 4

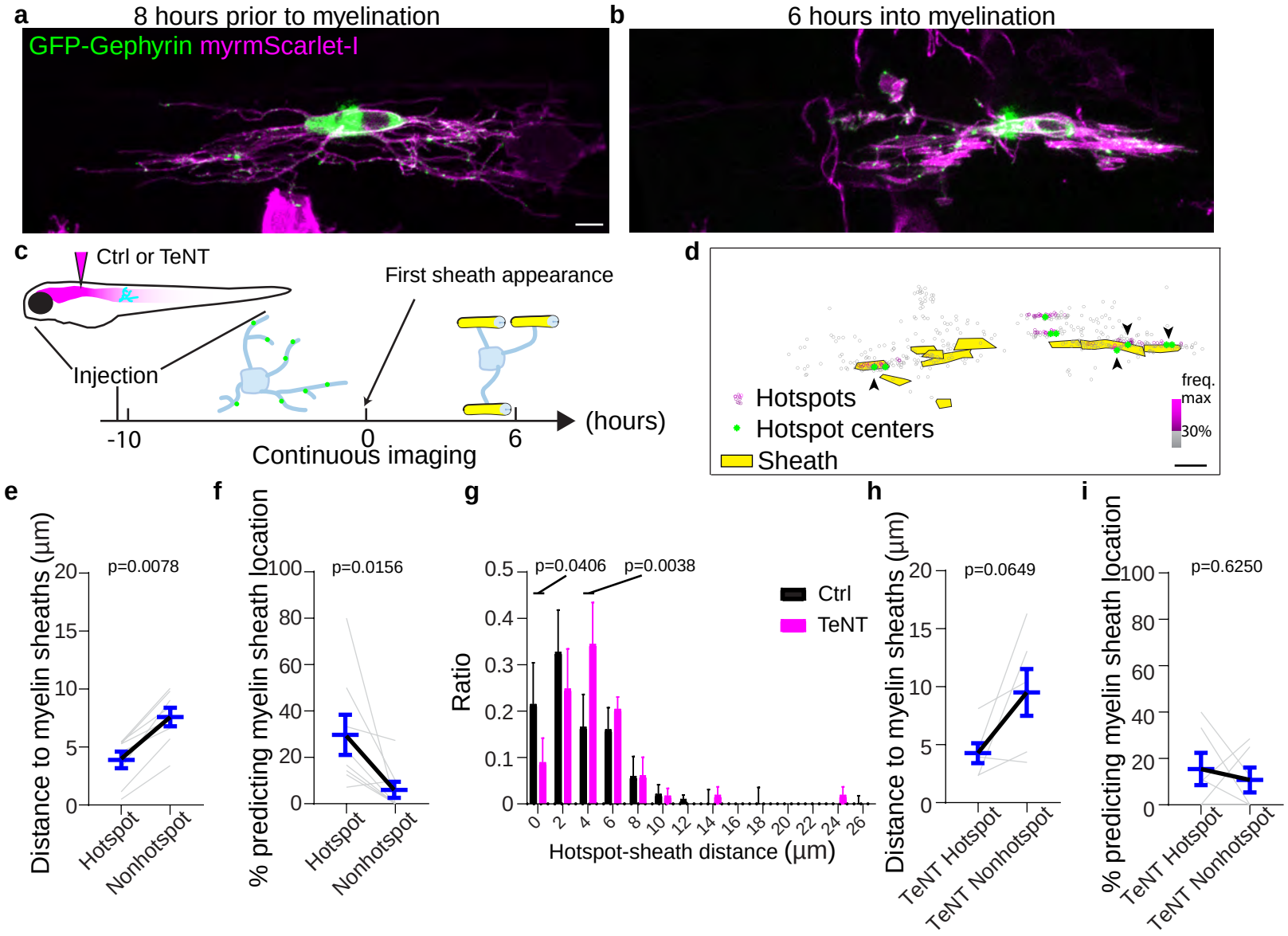
a
8 hours prior to myelination
GFP-Gephyrin myrmScarlet-I
b
6 hours into myelination
c
Ctrl or TeNT
First sheath appearance
Injection
-10
0
6
(hours)
Continuous imaging
d
Hotspots
Hotspot centers
Sheath
freq.
max
30%
e
Distance to myelin sheaths (µm)
p=0.0078
Hotspot
Nonhotspot
f
% predicting myelin sheath location
p=0.0156
Hotspot
Nonhotspot
g
Ratio
p=0.0406
p=0.0038
Ctrl
TeNT
Hotspot-sheath distance (µm)
h
Distance to myelin sheaths (µm)
p=0.0649
TeNT Hotspot
TeNT Nonhotspot
i
% predicting myelin sheath location
p=0.6250
TeNT Hotspot
TeNT Nonhotspot

Figure 5

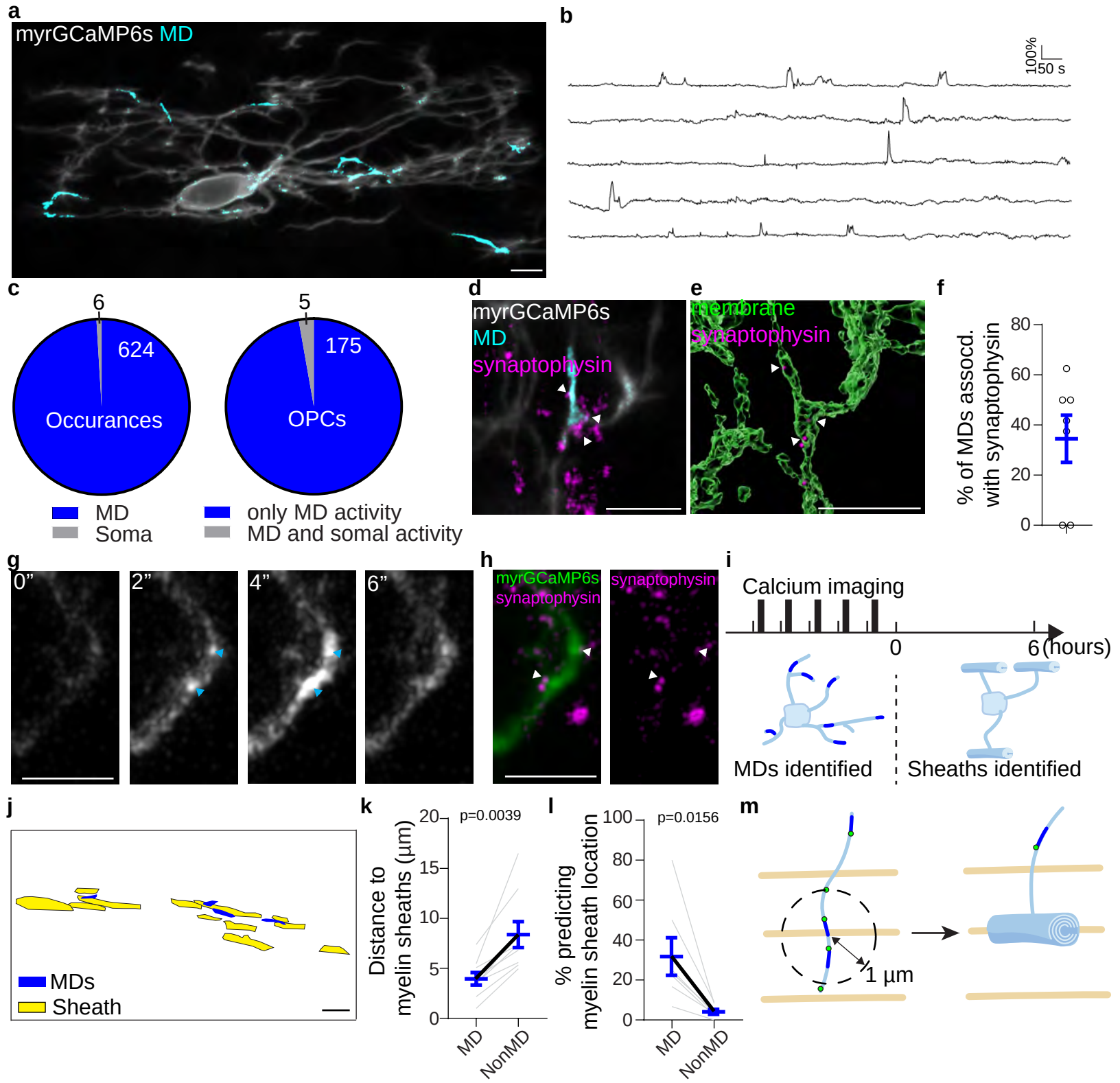
a
myrGCaMP6s MD
b
100%
150 s
c
6
624
Occurances
5
175
OPCs
MD
Soma
only MD activity
MD and somal activity
d
myrGCaMP6s
MD
synaptophysin
e
membrane
synaptophysin
f
% of MDs assocd. with synaptophysin
80
60
40
20
0
g
0”
2”
4”
6”
h
myrGCaMP6s
synaptophysin
synaptophysin
i
Calcium imaging
0
6 (hours)
MDs identified
Sheaths identified
j
MDs
Sheath
k
Distance to myelin sheaths (µm)
p=0.0039
20
15
10
5
0
MD
NonMD
l
% predicting myelin sheath location
p=0.0156
100
80
60
40
20
0
MD
NonMD
m
1 µm

Figure 6

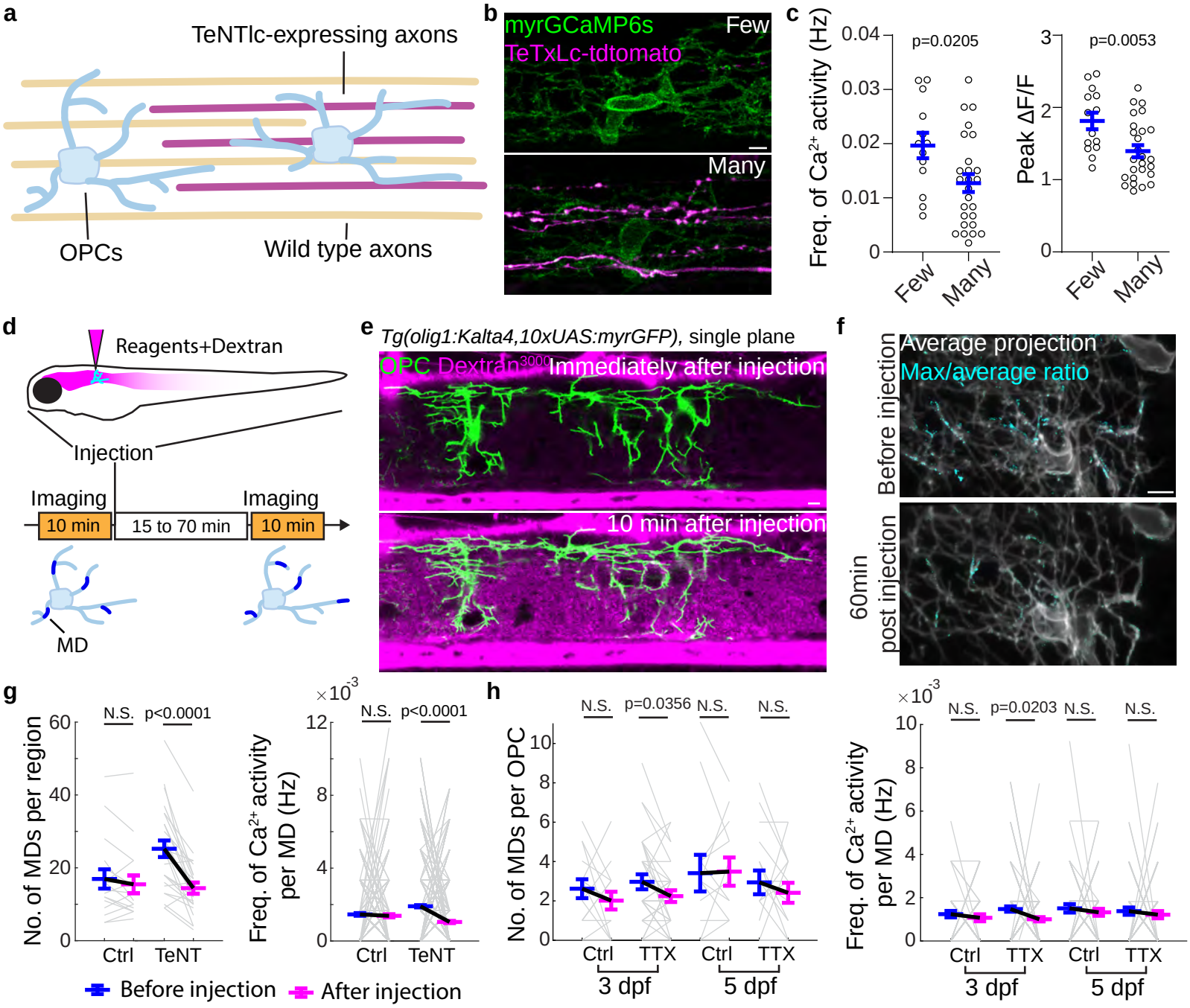
a
TeNTlc-expressing axons
OPCs
Wild type axons
b
myrGCaMP6s
TeTxLc-tdtomato
Few
Many
c
Freq. of Ca2+ activity (Hz)
p=0.0205
Peak ΔF/F
p=0.0053
Few
Many
d
Reagents+Dextran
Injection
Imaging
10 min
15 to 70 min
Imaging
10 min
MD
e
Tg(olig1:Kalta4,10xUAS:myrGFP), single plane
OPC Dextran3000
Immediately after injection
10 min after injection
f
Average projection
Max/average ratio
Before injection
60min post injection
g
No. of MDs per region
N.S.
p<0.0001
Ctrl
TeNT
Freq. of Ca2+ activity per MD (Hz)
×10-3
Before injection
After injection
h
No. of MDs per OPC
N.S.
p=0.0356
Ctrl
TTX
3 dpf
5 dpf
Freq. of Ca2+ activity per MD (Hz)
p=0.0203

Figure 7

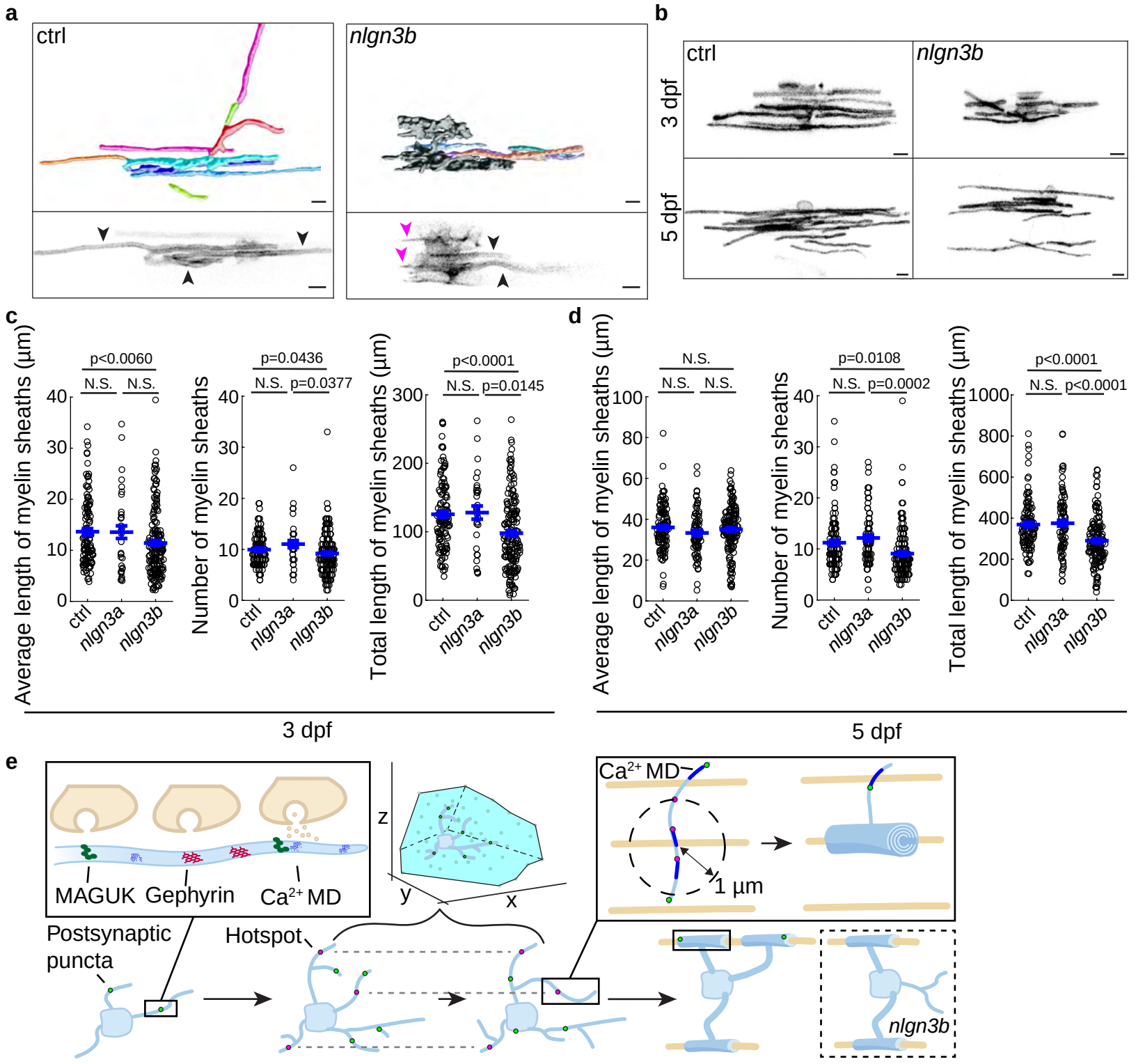
a
ctrl
nlgn3b
b
ctrl
nlgn3b
3 dpf
5 dpf
c
Average length of myelin sheaths (µm)
p<0.0060
N.S.
N.S.
Number of myelin sheaths
p=0.0436
N.S.
p=0.0377
Total length of myelin sheaths (µm)
p<0.0001
N.S.
p=0.0145
ctrl
nlgn3a
nlgn3b
3 dpf
d
Average length of myelin sheaths (µm)
N.S.
N.S.
N.S.
Number of myelin sheaths
p=0.0108
N.S.
p=0.0002
Total length of myelin sheaths (µm)
p<0.0001
N.S.
p<0.0001
ctrl
nlgn3a
nlgn3b
5 dpf
e
MAGUK
Gephyrin
Ca2+ MD
z
y
x
Postsynaptic puncta
Hotspot
Ca2+ MD
1 µm
nlgn3b

Figure 8